Respiratory Droplet Resuspension Near Surfaces: Modeling and Analysis

Mehdi Nikfar [a], **Ratul Paul** [a], **Khayrul Islam** [a], **Meghdad Razizadeh** [a], **Anand Jagota** [b, c] **and Yaling Liu** [a, b *]

[a] *Department of Mechanical Engineering and Mechanics, Lehigh University, Bethlehem, Pennsylvania 18015, USA.*

[b] *Department of Bioengineering, Lehigh University, Bethlehem, Pennsylvania 18015, USA.*

[c] *Department of Chemical and Biomolecular Engineering, Lehigh University, Bethlehem, Pennsylvania 18015, USA.*

[*]Corresponding author, email: yal310@ lehigh.edu.

Abstract

Knowing the environmental spreading pathway of COVID-19 is crucial for improving safety practices, particularly for health care workers who are more susceptible to exposure. This paper focuses on possible secondary transmission due to resuspension of virus-laden droplets from common surfaces, which several studies have shown to be possible under external disturbances. Such disturbances could be body motion during walking, running, clothes removal, or airflow in the environment. In this paper, a three-dimensional two-phase model is utilized to study respiratory droplet resuspension dynamics on various surfaces due to sudden agitation. The velocity range and variation during walking, surgical glove removal, and dropping an object are studied experimentally. A parametric study is performed to characterize the effects of droplet size and surface wettability on the minimum initial droplet velocity required for detachment from surfaces. The results are reported as average droplet velocity during the detachment process, total detachment time, and detached droplet volume. The obtained results indicate that respiratory droplets larger than 200 μm can detach from typical surfaces due to normal daily activities. Droplets are partially separated from the hydrophilic surface with contact angle $\leq 90^{o}$, while the entire droplet is detached from hydrophobic surfaces with contact angle $> 90^{o}$. Furthermore, the minimum initial droplet velocity to induce the resuspension depends on the droplet size. Droplet velocity immediately after detachment is a function of droplet size, initial droplet velocity and surface wettability. Bigger droplets have larger detached volume percentage as well as higher velocity after detachment, compared to smaller droplets. Finally, a higher initial velocity is needed to separate droplets from hydrophilic surfaces as compared to hydrophobic surfaces. In accordance with the results, the droplet minimum initial velocity to cause detachment is 2 ms^{-1}, while our experiments show that surface velocity can reach up to 3 ms^{-1} during normal human activities. We also develop an analytical model to predict the required kinetic energy to detach droplets from different surfaces, which is in good agreement with numerical results. The mechanism of droplet detachment is dictated by a competition between droplet kinetic energy induced by surface motion and surface energy due to droplet-surface interaction as well as droplet-vapor and surface-vapor interaction. We believe that results of this fundamental study can potentially be used to suggest proper surface wettability and safe motion that reduce respiratory droplet resuspension from various surfaces.

Keywords: COVID-19, Respiratory Droplets, Pathogen-Laden, Resuspension.

1. Introduction

A principal mode for transmission of respiratory infections such as coronavirus (COVID-19), severe acute respiratory syndrome (SARS), Spanish flu (H1N1), and influenza is by virus-laden fluid particles (i.e., droplets and aerosols) that are created in the respiratory system of an infected person and expelled from the mouth and nose during breathing, talking, coughing, and sneezing [1]–[3]. The current outbreak of COVID-19 has led to over 100 million confirmed cases and over 2 million deaths worldwide as of February 2021. The major distinction between aerosol and a droplet is the former's ability to float for hours in the air. This phenomenon is often dictated by their size. Usually, a droplet reaches the ground due to gravity before it poses any threat to be transmitted by breathing. But when the size of the droplet is very small, it evaporates before hitting the ground and leaves the nuclei of the droplet floating in the air for hours [4]. Previous studies demonstrated that the respiratory droplet size is on the order of O(10) μm to O(100) μm [5]–[11]. Han et al. [12] measured the droplet size distribution in 44 sneezes of 20 healthy subjects, and reported 360 μm as the mean diameter for respiratory droplets. However there is a grey area in defining the cutoff size of droplets which generate aerosols: it has been reported that droplets larger than 100 μm most probably deposit and contaminate surrounding surfaces [5]–[11]. Because the majority of respiratory droplets are larger than 100 μm [12], understanding the dynamics of respiratory droplets on surfaces is important.

Despite using personal protective equipment (PPE) while attending to the patients, health care workers (HCWs) accounted for over 20% of the cases during the outbreak of SARS in 2003. After the outbreak of COVID-19, many studies have been published as a guideline for appropriate level of protection required to safely attend to the patients [13], [14]. The dynamics of aerosol and droplets during coughing or sneezing and efficiency of different protective equipment have been studied with high speed imaging and particle detection [15]–[19]. Yet, droplets remaining on the PPE pose a threat of secondary transmission. A study of influenza virus infectivity on PPE surfaces such as rubber gloves, N95 respirator, surgical mask and Dupont Tyvek® with controlled deposition showed infectivity for up to 24 hours [20]. A study on trained health workers in Canada showed signs of contamination in selected regions of skin and dress after removing PPE even after following the protocol given by Public Services Health and Safety Association (PSHSA). Similar study conducted in the University of North Carolina Hospital among ten HCWs shows sign of contamination on the right and left hand, shirt, pant and face [21]. In the current outbreak of COVID-19, the shortage of PPE has encouraged the idea of using the same PPE for multiple patient encounters [22]. This makes the secondary transmission even more critical.

The flow physics and direct suspension of respiratory droplets from coughing and the subsequent contamination has been the focus of many studies [23], [24]. In these studies, nonlinear Navier-Stokes equations are solved using different algorithms available in computational fluid dynamics (CFD) field to investigate pathogen transmission in different environments such as hospitals, teaching buildings, supermarkets, etc. Finite difference method (FDM), finite element method (FEM) and finite volume method (FVM) have commonly used to capture the movement mechanism of respiratory droplets. In these simulations, to track respiratory droplet trajectories, they are treated as a point in the context of a discrete phase [23], [24]. These mentioned approaches are not able to model the droplet deformation. Modeling and analysis of droplet behavior on vibrating surfaces have also received great attention because of its applications in different fields such as self-cleaning glass [25] and heat transfer in heating, ventilation, and air conditioning applications [26]. For example, Wilkes et al. [27] used Galerkin/finite element to analyze the force oscillation of a pendant droplet on a rod with a fixed contact line. They investigated the effect of Reynolds number (Re), gravitational Bond number (G) and droplet size on the drop deformation. The detachment of small oil droplets from metal substrates embedded in an aqueous medium was carried out by Chatterjee [28]. They showed that buoyancy-induced breakup is the main reason for the droplet removal. They presented an analytical solution for droplet shape variations on the surface. Shin and Lin [29] also developed analytical and experimental approaches to model droplet shape deformation and detachment conditions on a vibrating flat surface. They qualitatively identified the competition between kinetic and surface energies as determining the detachment condition during oscillatory motion. The difference between experimental and analytical results were related to several factors such as contact line friction, nonlinear wall adhesion, and experimental uncertainty. Drop motion caused by vertical vibration of an inclined plate was studied by Sartori et al. using diffuse interface method [30]. It was shown increasing the oscillating amplitude moves the drop upward against gravity. A study on the detachment behavior of micron-sized droplets shows normal and tangential forces have different effects on the droplet. Increasing normal force results in partial droplet detachment, which is measured by the volume change, while increasing tangential force results in complete detachment [31]. There are several other studies of droplet contact line motion [32] using Methods such as Lattice Boltzmann (LBM) [33], [34], Surface Evolver [35], Cahn–Hilliard/Navier–Stokes (CHNS) [36], and Volume of Fluid (VOF) [37]. However, to the best of our knowledge, the detachment of a pendant or sessile droplet from surfaces due to its initial velocity has not been studied comprehensively nor linked to resuspension of respiratory droplets.

Different studies show that secondary transmission is possible due to resuspension of virus-laden droplets from PPE surfaces under external disturbance [4], [21], [38]–[41]. Such disturbance could be body motion during walking, running, clothes removal or airflow in the environment. It has been confirmed that virus aerosol deposition on protective apparel or the floor surface and their subsequent resuspension is a potential transmission pathway of COVID-19 in hospitals [42]. Initial studies [43]–[46] show that environmental conditions such as humidity and temperature as well as surface properties, e.g., surface chemistry, roughness, and wettability have significant effects on the evolution of aerosols and droplets. The dynamics of the respiratory droplets on common PPE surfaces and the secondary exposure risk due to resuspension of those droplets have not been systematically evaluated. A better understanding of droplet resuspension from PPE and various surfaces during daily activities can help minimize secondary droplet contamination. In this paper, a three-dimensional two-phase isothermal model is used to model the respiratory droplet resuspension near surfaces with different wettability. The droplet minimum initial velocity to trigger the detachment process is obtained for droplets with various sizes on different surfaces. The results are presented in the form of droplet average velocity during detachment process and droplet volume detached from surfaces.

2. Problem Description

As shown schematically in Figure 1 (a), droplets larger than a critical size (~100 μm) deposit faster than they evaporate and contaminate surrounding surfaces [6]. Droplets smaller than this size evaporate more quickly than they settle, forming droplet nuclei that can stay airborne for hours and be transported over long distances. Larger droplets can deposit on different surfaces such as the floor, table and PPE. The motion of the mentioned surfaces can result in either complete or partially droplet resuspension. The surface wettability and surface motion both dictate the detachment dynamics. Figure 1 (b) is a schematic view of the computational setup for a virus-laden droplet on a stationary surface. In the simulation, the surface is considered as a flat, stationary, wall and the rest of the boundaries are defined as pressure outlets with zero as the gauge pressure. The surrounding fluid is air at 300 K, which is assumed to be stationary at the pressure of 101.3 kPa. Due to the similarity of saliva and water, thermophysical properties of water are utilized in this paper for the respiratory droplets [47]–[51]. Density and viscosity for both air and droplet liquid, and air-droplet surface tension are listed in Table 1.

As Figure 1 (b) illustrates, the droplet is initially a spherical cap with d as the diameter, attached to the surface with a contact angle θ_w. Considering the contact angle, we stabilized the droplet structure for adequate time steps without initial velocity to achieve the droplet's actual shape on the surface. Afterward, an initial velocity is applied on the droplet. This corresponds to sudden arrest of a moving substrate along with a droplet on it. Viruses are encapsulated inside the respiratory droplet. Because the virus particle is very small in size (~100 nm) compared to the respiratory droplets (at least ~10 microns) with low concentration, in this study, we do not model the virus explicitly. The modeling domain size in each direction is two times the droplet diameter ($2d$). The problem formulation can be found in supplementary materials.

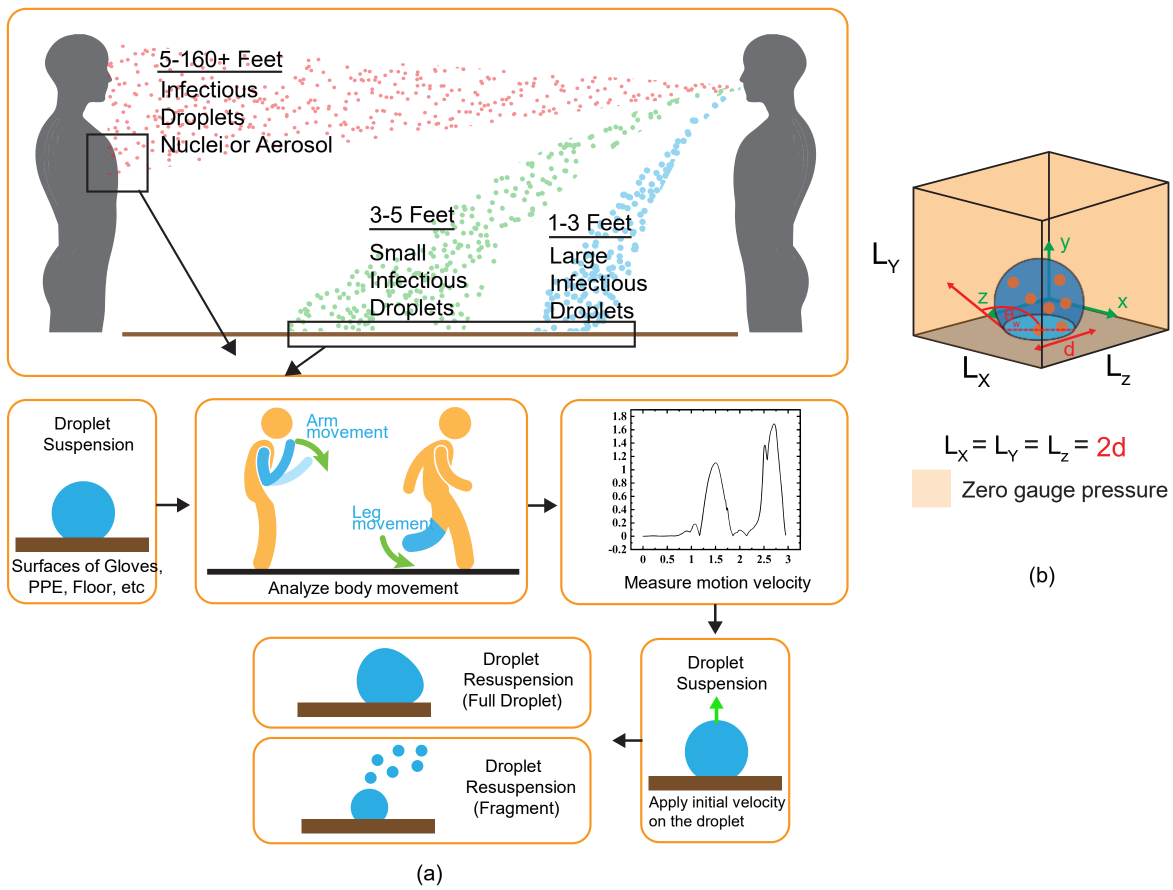

Figure 1: (a) Travel length of the infectious droplet and droplet nuclei, and their interaction with surfaces (b) A schematic view of the computational setup

Table 1: Air and droplet properties used in this study

	Air (Primary Phase)	**Droplet (Secondary Phase)**
Viscosity (kg/ms)	$\mu_a = 1.7894 \times 10^{-5}$	$\mu_l = 0.001003$
Density (kg/m^3)	$\rho_l = 1.225$	$\rho_l = 998.2$
Surface Tension (N/m)	-	$\sigma = 0.073$

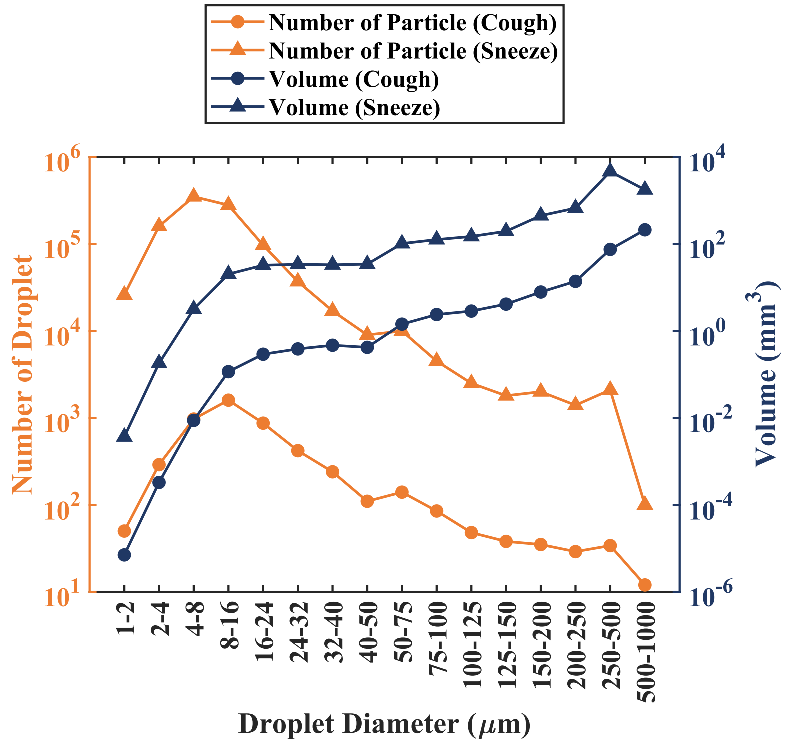

Figure 2: Respiratory droplet diameter, number and corresponding volume in one cough or sneeze [6].

3. Experimental Procedure

The initial droplet velocity was estimated based on an experiment conducted by attaching an accelerometer with 250 Hz data recording speed to the forearm and right leg of a person (Male, 5'8" height), and attaching it to a dropping object (face shield). The movements were based on possible activities that can generate large velocity in a healthcare environment. We recorded the accelerometer sensor data while removing a surgical glove, walking, and dropping an object. The corresponding absolute velocities were obtained by numerical integration from recorded accelerations in each direction using MATLAB. The computed velocities (Figure 3) show that the forearm can generate an absolute velocity up to 2.2 ms^{-1} while removing surgical gloves. The leg can generate a velocity up to 1.7 ms^{-1} while walking in a regular manner. Dropping an object can reach a velocity up to 3.1 ms^{-1}. The velocity range measured here will be used as the droplet initial velocity in later sections.

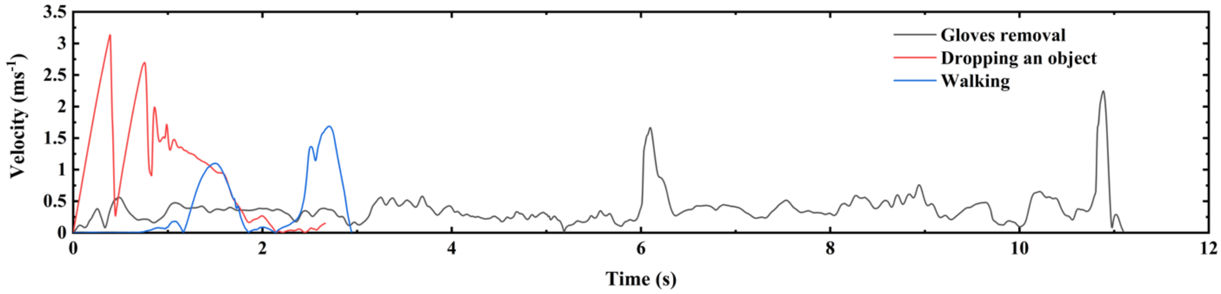

Figure 3: Range of velocity during walking, removing surgical gloves, and dropping an object

4. Numerical Procedure

ANSYS-Fluent 19.0 (ANSYS, Inc., Pennsylvania, USA) is selected to perform the numerical procedure on a structured computational grid. Following the initialization of pressure, velocity, and volume fraction in the entire computational domain, the droplet initial velocity and water volume fraction ($\alpha_l = 1$) is patched to the droplet region on the wall specified for the droplet initial condition. The explicit volume fraction is used to capture the interface. A second-order upwind scheme is implemented to enhance the method accuracy. A geometric reconstruction approach named Geo-Reconstruct in ANSYS Fluent is also applied to calculate the face fluxes. In this approach, for the computational cells close to the interface and between two faces, a piecewise-linear scheme assumes a linear interface slope within those cells. Geo-Reconstruct option is the most precise approach in ANSYS-Fluent for multiphase flows. The well-known SIMPLE (semi-implicit method for pressure linked equations) method [66] is used for pressure–velocity coupling. In the SIMPLE algorithm, the continuity equation is converted to an equation for the pressure, and PRESTO (staggering pressure option) is utilized to solve it. Moreover, for gradient calculations, the least-squares cell-based method is chosen to minimize computation time and guarantee sufficient accuracy. A first-order implicit method is selected for time discretization. A time step size of 10^{-6} s is used to capture the details of the droplet detachment dynamics from the surface. The selected mesh size and time steps must satisfy the maximum Courant number condition ($\frac{V\Delta t}{\Delta x} \leq 0.25$). V is the droplet initial velocity (ms^{-1}), Δt is the time step (s) and Δx is the grid size (m). The calculations were completed by a 64-bit, Intel Core i9-9900K CPU, 3.60 GHz, 32 Gb RAM, Windows 10 Professional computer, and the CPU time of calculation was up to 1 hour.

5. Computational Grid Independence

To determine a proper computational mesh for the numerical simulations, a grid independence study is conducted to detach a droplet with d = 400 μm diameter from a surface with a contact angle equal to 50º, a typical contact angle as listed in Table 1S. A typical computational grid along with droplet region used in this study are shown in Figure 4. As the figure shows, the computational grid is uniform and composed of hexahedron elements. The droplet initial velocity is equal to the maximum velocity obtained experimentally, i.e., $V = 3\ ms^{-1}$. As described earlier, the domain size is $2d \times 2d \times 2d$. Five different uniform grids, with the mesh size of $d/10$, $d/15$, $d/20$, $d/25$, and $d/40$ are employed for the numerical calculations. The time step is kept constant and equal to 10^{-6} s for all the simulations. The droplet average velocity variations over time are displayed in Figure 5. The average velocity is plotted from t = $2 \times 10^{-5}\ s$ after applying the initial velocity to avoid showing sharp velocity reduction immediately after applying the initial velocity. As the figure shows, for mesh sizes smaller than $d/25$, no further improvement is achieved by mesh refinement. Therefore, a uniform grid with $d/25$ mesh size is used to perform all the subsequent simulations in this paper.

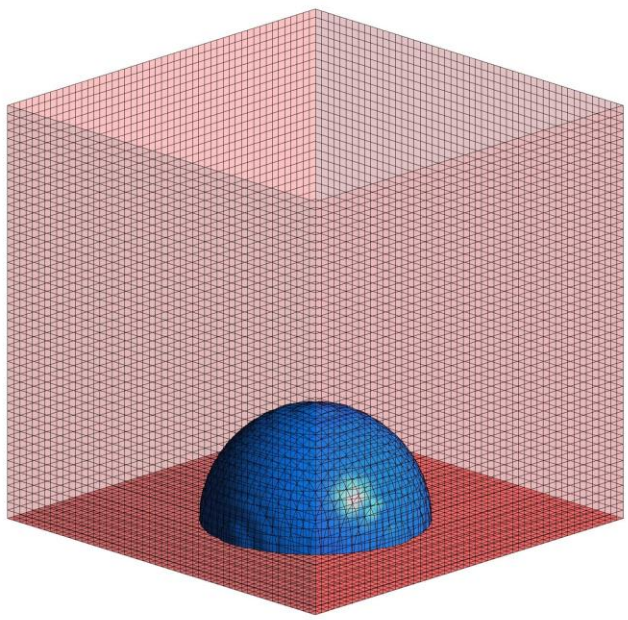

Figure 4: A typical computational grid

Journal of Applied Physics

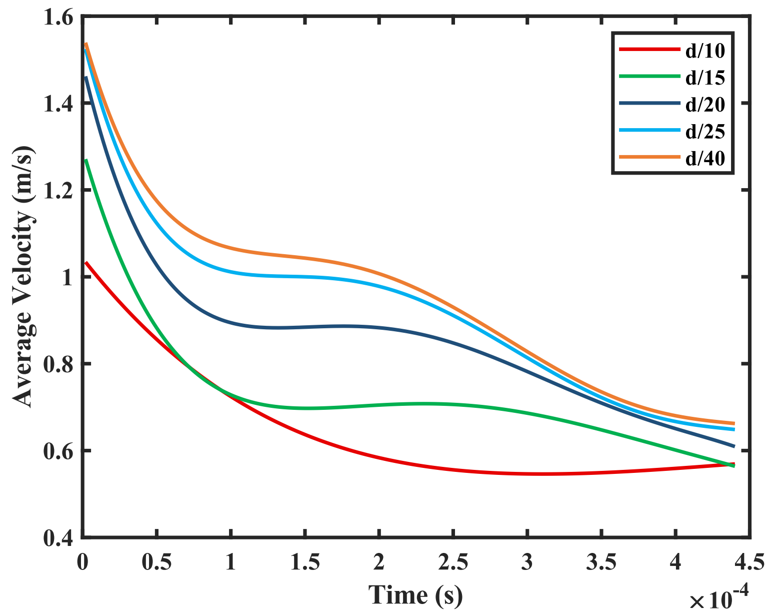

Figure 5: Average droplet velocity simulated under different computational grids

6. Results and Discussion

Having obtained the proper computational grid size, we analyze the effect of droplet size and surface wettability on the minimum initial droplet velocity to detach the droplet from various surfaces. In the following subsections, we first investigate the impact of the droplet size on the detachment process, and then we focus on the surface wettability role.

6.1. Droplet size

To understand how the droplet size influences minimum detachment velocity, the detachment process is modeled for droplets with 50 μm, 200 μm, 400 μm, and 800 μm diameters. In all the simulations, the contact angle is kept constant at 50º, the average value listed in Table 1S. To find the droplet minimum initial velocity for observing the detachment, the droplet initial velocity is increased by 0.1 ms^{-1} until the detachment is observed. Figure 6 shows the minimum velocity required for detaching droplets with different sizes. As the figure illustrates, droplets smaller than 200 μm cannot be detached due to the activities mentioned in section 4. For example, a 50 μm droplet needs initial velocity of 7.9 ms^{-1} to detach, which is well above the 3.1 ms^{-1} maximum value measured experimentally. Among those that can be detached within the normal velocity range, the required velocity for 200 μm droplet is larger than others. In this case, the droplet mass is small and higher initial velocity should be applied to generate required kinetic energy to detach the droplet. With increased droplet size, the required initial velocity decreases because the droplet mass increases, and lower velocity can lead to the disassociation.

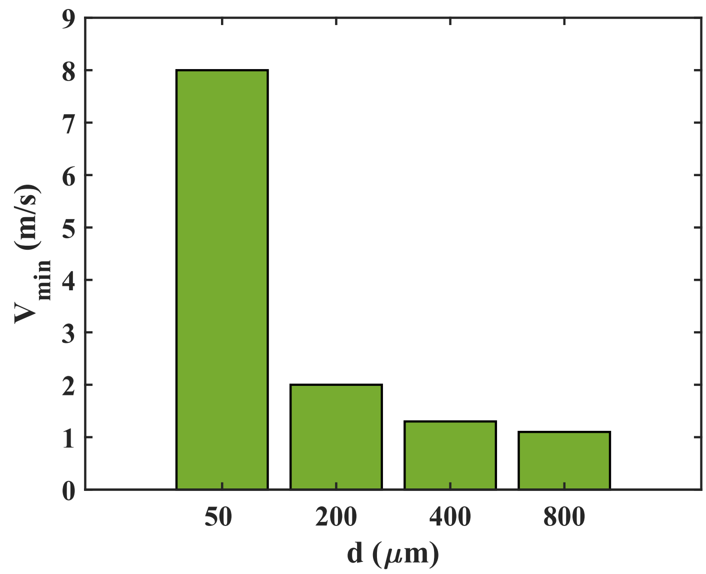

Figure 6: Minimum velocity required for the detachment for different droplet sizes

The time-sequence snapshots of the simulations are displayed in Figure 7. As the figure shows, in all the cases, the droplet detaches partially. Indeed, the initial velocity cannot overcome the adhesion between droplet and wall for total detachment. Moreover, Figure 7 shows that larger droplets detach slower due to the larger displacement required for detachment. The droplet average velocity during the removal process is plotted in Figure 8 (a). In all the cases, the average velocity decreases over time because, as we will discuss in next section, the droplet kinetic energy is converted to surface potential energy during detachment process. Moreover, Figure 8 (a) shows that the terminal velocity of droplet after detachment depends on both the droplet size and initial velocity. For the 800 μm droplet, the terminal velocity is higher than the other two droplets because it is easier for larger droplets to break into pieces during detachment. Since the droplet detachment happens partially, the detached droplet volume percentage is plotted in Figure 8 (b). As the plot shows, the detached volume percentage is higher in larger droplets since less energy is consumed to split the droplet.

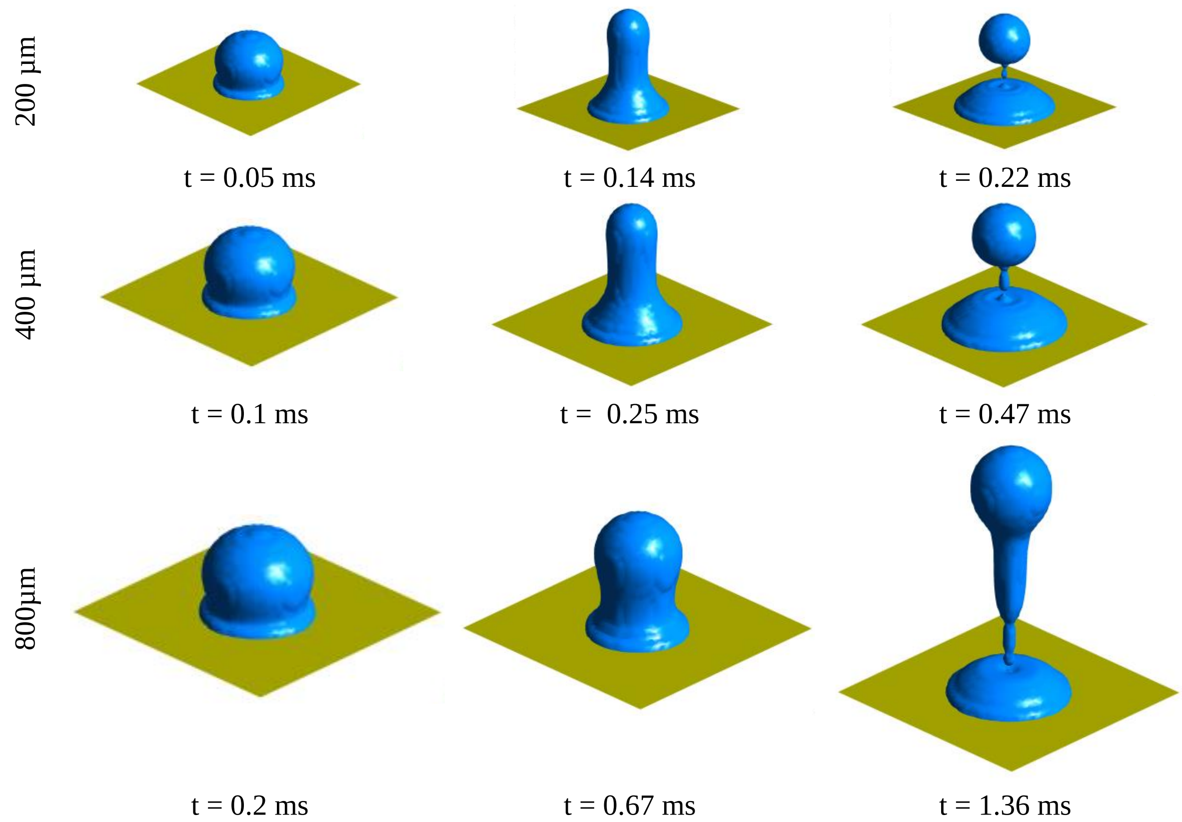

Figure 7: Droplet detachment process near the surface for droplets of different sizes with $\theta_w = 50°$

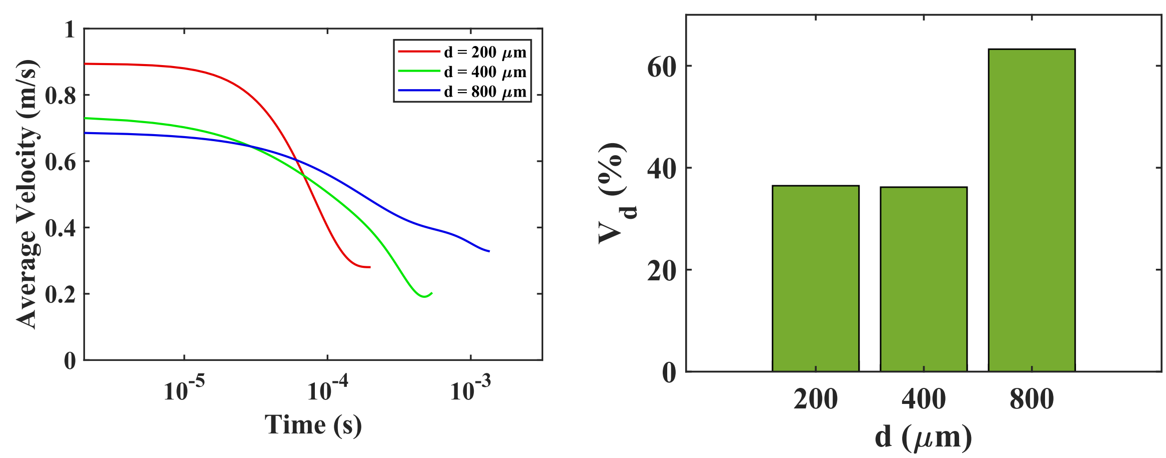

(a) (b)

Figure 8: (a) Average droplet velocity over time and (b) Volume percentage of detachment droplet, for droplets of various sizes at $\theta_w = 50°$

After obtaining the minimum velocity for the detachment of droplets with different sizes, the above simulations are repeated for droplet initial velocity equal to 2.5 ms^{-1} to know how the droplets behave when they experience the same initial velocity higher than minimum initial velocity. Figure 9 (a) illustrates the droplet average velocity during resuspension. As it can be observed, removal process takes longer time for larger droplets, and the droplet terminal velocity is higher. The droplet detachment volume percentage is also shown in Figure 9 (b). As shown in the figure, for 800 μm droplets, a significantly larger portion of the droplet is detached from the surface. It should be mentioned that while the detached volume percentage for 400 μm droplet is smaller than 200 μm droplet, the total detached volume is still larger.

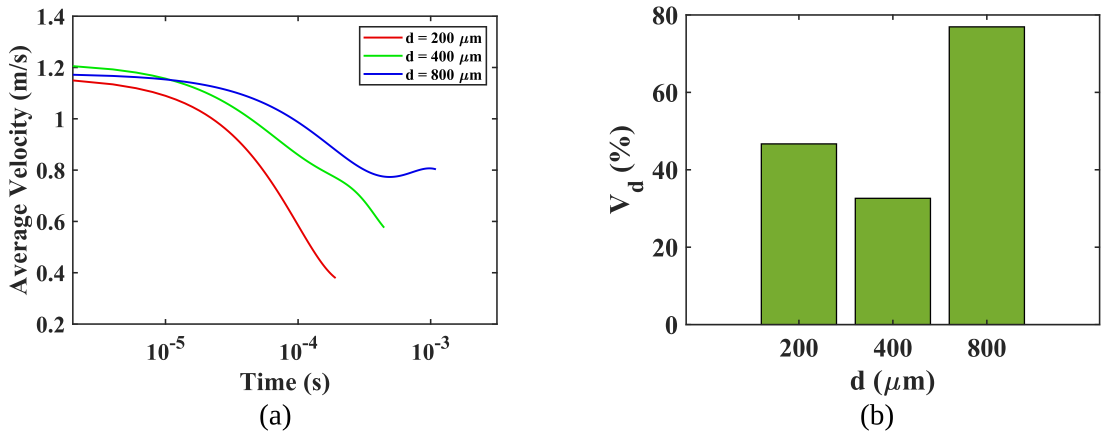

Figure 9: (a) Average droplet velocity over time and (b) detached droplet volume percentage, for various droplet sizes at $\theta_w = 50°$ and V = 2.5 ms^{-1}

6.2. Surface Wettability

Surfaces with contact angles of 5º, 50º, and 100º are modeled to analyze the effect of surface wettability on the value of minimum velocity for the detachment. These three contact angles cover the entire range of contact angle listed in Table 1S. In all the test cases, the droplet diameter is 400 μm. To obtain the minimum initial droplet velocity to induce the detachment, the droplet initial velocity increases by 0.1 ms^{-1} until the detachment is observed. Minimum velocity for detachment from different surfaces is plotted in Figure 10. It can be observed that the minimum velocity increases with decreased contact angle because the interaction between droplet and hydrophilic surface is stronger than that with hydrophobic surfaces. All the velocities are in the range of observed velocities in the experiment.

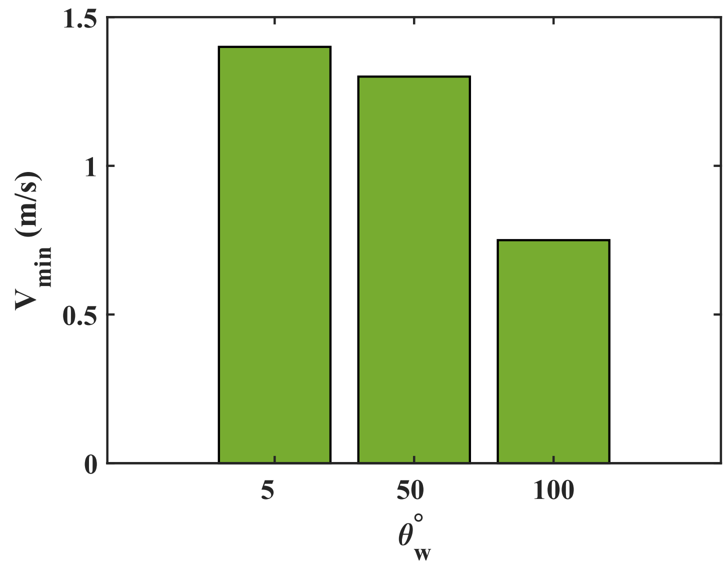

Figure 10: Minimum velocity required for the detachment from surfaces with various wettability

To analytically show dependency of the minimum initial velocity on contact angle, we imagine a sessile droplet at its equilibrium shape sitting on a stationary substrate (Figure 11 (a)). The droplet is small enough that we may neglect gravity. The droplet and substrate are both traveling together at velocity, *v*. At time *t* = *0*, we suddenly stop the motion of the rigid substrate. The drop will now change its shape due to the relative velocity with respect to the stationary substrate. Clearly, if the velocity is large enough or if the droplet barely wets the surface, then it will be easier to resuspend the droplet. Here we develop a simple analytical model that predicts the condition under which this sessile droplet will resuspend. The condition for resuspension is that the kinetic energy of the liquid must at least be equal to the increase in surface energy due to change of its initial equilibrium shape to one in which contact angle equals π. We assume that, as the droplet deforms, it adopts a series of shapes each of which is a spherical cap under the constraint of constant volume (Figure 11 (a)). There are several ways we can write the volume and surface of aspherical cap shown in Figure 11 (b). We will use formula based on contact angle θ, and radius of spherical cap, *r*:

$$V = \frac{\pi}{3} r^3 (2 - 3cos\theta + cos^3\theta); r = \left[\frac{3}{\pi} \frac{V}{2 - 3cos\theta + cos^3\theta}\right]^{1/3}, \quad (1)$$

$$A_{LV} = 2\pi r^2 (1 - cos\theta), \quad (2)$$

$$A_{SV} = \pi r^2 sin^2\theta. \quad (3)$$

The total energy of the system is the sum of kinetic and potential energies. At the start of the process, all of it is kinetic energy. At the end of the process all of it is the surface potential energy. The surface potential energy is:

$$G = \gamma_{LV} A_{LV} + (\gamma_{SL} - \gamma_{SV}) A_{SL}, \tag{4}$$

where, γ_{LV}, γ_{SL}, and γ_{SV} are the surface energies of the liquid-vapor, solid-liquid, and solid-vapor interfaces, respectively, and A_{LV}, A_{SL} are the areas of the liquid-vapor and solid-vapor interfaces, respectively. Replace r in Eqs (2) and (3) by its expression in Eq. (1) in terms of constant volume V, and angle θ. Then substitute the resulting expressions into Eq. (4) to get:

$$G(\theta) = (72\pi)^{\frac{1}{3}} \gamma_{LV} \left(\frac{V}{2 - 3cos\theta + cos^3\theta}\right)^{\frac{2}{3}} (1 - cos\theta) + (9\pi)^{\frac{1}{3}} (\gamma_{SL} - \gamma_{SV}) \left(\frac{V}{2 - 3cos\theta + cos^3\theta}\right)^{\frac{2}{3}} sin^2\theta. \tag{5}$$

The equilibrium shape is found by

$$\frac{dG(\theta)}{d\theta} = 0 \therefore\ cos\theta_w = \frac{\gamma_{SV} - \gamma_{SL}}{\gamma_{LV}}. \tag{6}$$

This is Young's equation for the equilibrium contact angle. The condition for maximum extension (maximum contact angle, θ_f) is that the change in potential energy equals the initial kinetic energy, or,

$$\frac{1}{2} \rho V v^2 \geq\ G(\theta_f) - G(\theta_w). \tag{7}$$

The resuspension condition is that $\theta_f \to \pi$ or:

$$\frac{1}{2} \frac{\rho V^{1/3} v^2}{\gamma_{LV}} \geq\ (36\pi)^{1/3} - (72\pi)^{\frac{1}{3}} \left(\frac{1}{2 - 3cos\theta_w + cos^3\theta_w}\right)^{\frac{2}{3}} (1 - cos\theta_w) + (9\pi)^{\frac{1}{3}} \left(\frac{1}{2 - 3cos\theta_w + cos^3\theta_w}\right)^{\frac{2}{3}} cos\theta_w sin^2\theta_w. \tag{8}$$

Defining the right-hand side (RHS) of Eq (8) as a dimensionless surface energy, and the left-hand side (LHS) as a dimensionless kinetic energy (k), we can plot dimensionless kinetic energy $\boldsymbol{k}$ as a function of contact angle θ_w as shown in Figure 12. In this figure, for dimensionless kinetic energy below the phase separation line, no detachment will happen. However, for the dimensionless kinetic energy above the phase separation line, resuspension occurs. Figure 12 also compares the analytical solutions with numerical results reported in previous sections. As the figure shows, except for small contact angles, other results are in a good agreement. For small contact angles, as we will explain later on, only a small portion of the droplet detaches due to the applied velocity. However, the analytical solution assumes complete detachment of droplet, thus is not expected to be applicable for small contact angles and partial detachment.

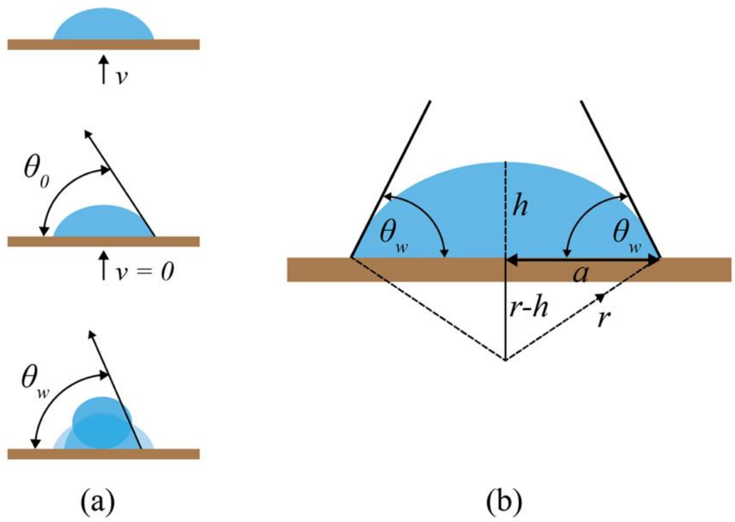

Figure 11: Schematic view of a droplet on a rigid substrate: (a) Equilibrium process, (b) Equilibrium shape

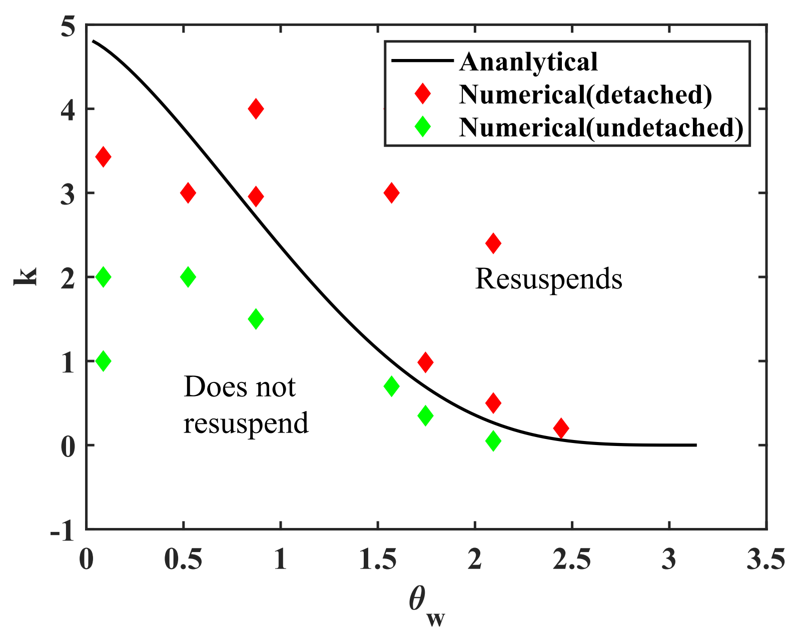

Figure 12: Comparison between analytical and numerical results for phase diagram of dimensionless kinetic energy versus contact angle

A few snapshots of the simulation of droplet detachment over time from surfaces with different contact angles are shown in Figure 13. As shown in the figure, with increased contact angle smaller amounts of the liquid are left on the surface. The average velocity variations of droplet with respect to time are depicted in Figure 14. As it can be observed the average velocity of droplet decreases over time because of conversion of kinetic energy to surface potential energy. The detached droplet volume percentage is also shown in Figure 14 (b). The droplet volume percentage detached from hydrophobic surface is larger than that from hydrophilic surfaces. This is in agreement with snapshots shown in Figure 13.

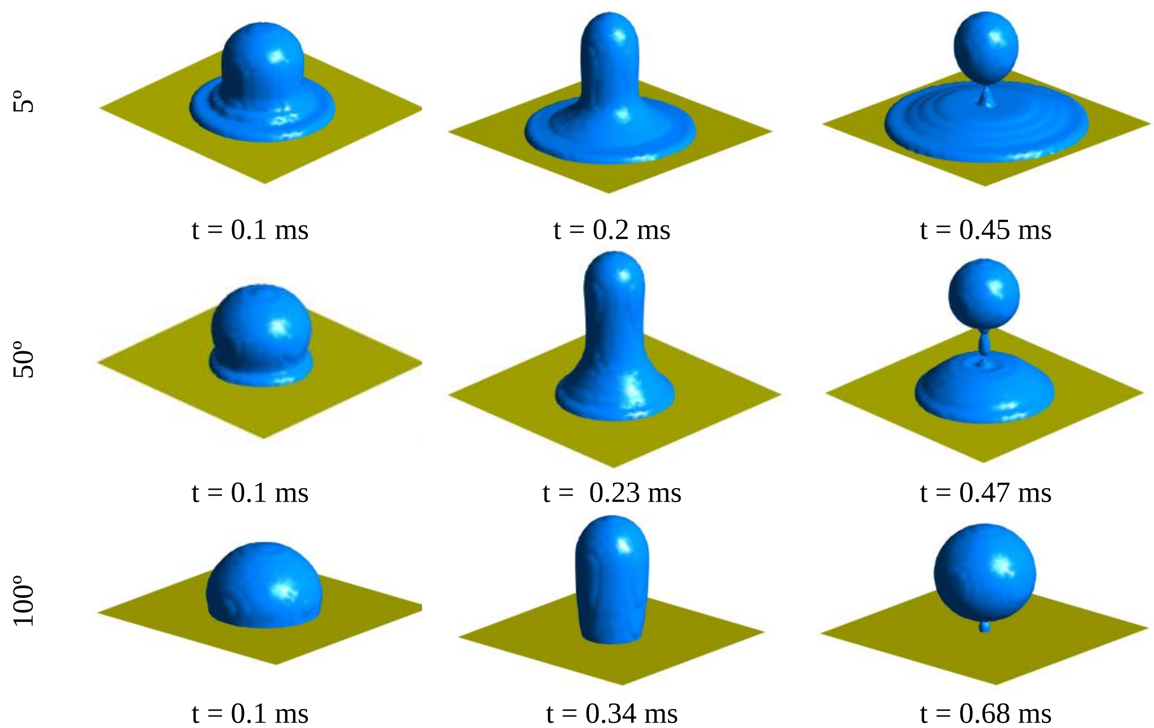

Figure 13: Detachment of a droplet with $d = 400\ \mu m$ diameter from surfaces with different wettability

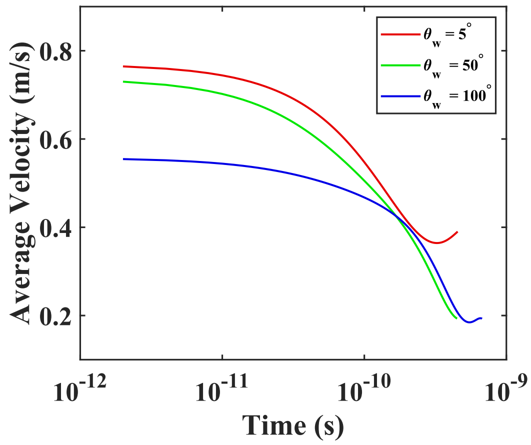

(a)

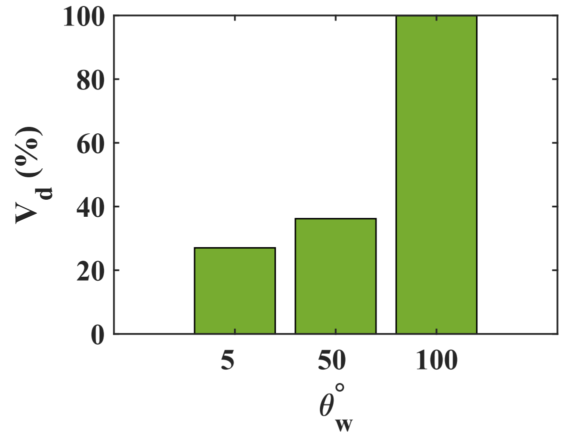

(b)

Figure 14: (a) Average droplet velocity over time and (b) detached droplet percentage, for a droplet with $d = 400\ \mu m$ diameter from different surfaces

7. Conclusion

A CFD and an analytical model were employed to quantify the effect of the droplet diameter and surface wettability on the minimum initial droplet velocity needed to detach the respiratory droplets from surfaces. The range of surface velocity was measured experimentally. The experimental results show that maximum velocity in typical human activities such as walking and dropping an object can reach 3 ms^{-1}. The numerical results show this range of velocity is sufficient for droplet detachment from various PPE surfaces. An analytical model was also developed to predict the required conditions for droplet detachment from different surfaces. The analytical model found that droplet detachment is determined by balance of dimensionless kinetic energy and surface energy, which agrees with numerical simulation. Generally, the results show that larger droplets on hydrophobic surfaces are more dangerous because relatively small initial velocity can remove larger part of the droplets from surfaces. Such results help understand possible shortcomings in the standard healthcare safety protocol that can cause potential secondary viral infection. Consequently, the results from this study might be used to suggest possible surface property modifications or alternative surface material choices to avoid droplet resuspension or to reduce droplet resuspension possibility. The results can also be extended to provide potential guidance on daily activity in different environment for enhanced prevention.

Supplementary Materials

See the supplementary materials for the problem formulation.

Author Contributions

M.N. designed research, performed research, analyzed data, and wrote the paper. R.P. designed research, performed research, and wrote the paper. K.I. performed research, analyzed data, and wrote the paper. M.R. analyzed data and wrote the paper. A.J. designed and directed research, performed research, analyzed data and wrote the paper. Y.L. designed and directed research, performed research, analyzed data, and wrote the paper.

Acknowledgment

The authors acknowledge this work's support from the National Science Foundation (NSF) grant of CBET 2039310.

Data Availability

The data that support the findings of this study are available from the corresponding author upon reasonable request.

References

[1] R. M. Jones and L. M. Brosseau, "Aerosol transmission of infectious disease," *J. Occup. Environ. Med.*, vol. 57, no. 5, pp. 501–508, 2015.

[2] S. Asadi, N. Bouvier, A. S. Wexler, and W. D. Ristenpart, "The coronavirus pandemic and aerosols: Does COVID-19 transmit via expiratory particles?," *Aerosol Science and Technology*, vol. 54, no. 6. pp. 635–638, 2020.

[3] L. Bourouiba, "Turbulent Gas Clouds and Respiratory Pathogen Emissions: Potential Implications for Reducing Transmission of COVID-19," *JAMA - J. Am. Med. Assoc.*, vol. 323, no. 18, pp. 1837–1838, 2020.

[4] C. Desrochers, "Are Nurses Protected ? Observing the risk of skin contamination when donning and doffing personal protective equipment , using a Canadian protocol by Chelsie Desrochers A thesis submitted in partial fulfillment of the requirements for the degree of Master," Laurentian University, 2017.

[5] R. Tellier, "Aerosol transmission of influenza A virus: A review of new studies," *J. R. Soc. Interface*, vol. 6, no. SUPPL. 6, Dec. 2009.

[6] M. Nicas, W. W. Nazaroff, and A. Hubbard, "Toward understanding the risk of secondary airborne infection: Emission of respirable pathogens," *J. Occup. Environ. Hyg.*, vol. 2, no. 3, pp. 143–154, Mar. 2005.

[7] C. Chen and B. Zhao, "Some questions on dispersion of human exhaled droplets in ventilation room: Answers from numerical investigation," *Indoor Air*, vol. 20, no. 2, pp. 95–111, Apr. 2010.

[8] X. Xie, Y. Li, A. T. Y. Chwang, P. L. Ho, and W. H. Seto, "How far droplets can move in indoor environments - revisiting the Wells evaporation-falling curve," *Indoor Air*, vol. 17, no. 3, pp. 211–225, 2007.

[9] J. Fiegel, R. Clarke, and D. A. Edwards, "Airborne infectious disease and the suppression of pulmonary bioaerosols," *Drug Discovery Today*, vol. 11, no. 1–2. pp. 51–57, Jan-2006.

[10] L. Morawska, "Droplet fate in indoor environments, or can we prevent the spread of infection?," in *Indoor Air*, 2006, vol. 16, no. 5, pp. 335–347.

[11] S. D. Judson and V. J. Munster, "Nosocomial transmission of emerging viruses via aerosol-generating medical procedures," *Viruses*, vol. 11, no. 10. MDPI AG, Oct-2019.

[12] Z. Y. Han, W. G. Weng, and Q. Y. Huang, "Characterizations of particle size distribution of the droplets exhaled by sneeze," *J. R. Soc. Interface*, vol. 10, no. 88, 2013.

[13] WHO, "Rational use of personal protective equipment for coronavirus disease 2019 (COVID-19) and considerations during severe shortages," 2020.

[14] T. M. Cook, "Personal protective equipment during the coronavirus disease (COVID) 2019 pandemic – a narrative review," *Anaesthesia*, vol. 75, no. 7, pp. 920–927, Apr. 2020.

[15] T. Oberg and L. M. Brosseau, "Surgical mask filter and fit performance," *Am. J. Infect. Control*, vol. 36, no. 4, pp. 276–282, May 2008.

[16] M. Loeb *et al.*, "Surgical mask vs N95 respirator for preventing influenza among health care workers: A randomized trial," *JAMA - J. Am. Med. Assoc.*, vol. 302, no. 17, pp. 1865–1871, Nov. 2009.

[17] O. Aydin, M. A. B. Emon, S. Cheng, L. Hong, L. Chamorro, and M. T. A. Saif, "Performance of Fabrics for Home-Made Masks Against the Spread of Respiratory Infections Through Droplets: A Quantitative Mechanistic Study," 2020.

[18] L. Bourouiba, E. Dehandschoewercker, and J. W. M. Bush, "Violent expiratory events: On coughing and sneezing," *J. Fluid Mech.*, vol. 745, pp. 537–563, Apr. 2014.

[19] H. Nishimura, S. Sakata, and A. Kaga, "A new methodology for studying dynamics of aerosol particles in sneeze and cough using a digital high-vision, high-speed video system and vector analyses," *PLoS One*, vol. 8, no. 11, p. e80244, Nov. 2013.

[20] H. Sakaguchi *et al.*, "Maintenance of influenza virus infectivity on the surfaces of personal protective equipment and clothing used in healthcare settings," *Environ. Health Prev. Med.*, vol. 15, no. 6, pp. 344–349, Nov. 2010.

[21] L. Casanova, E. Alfano-Sobsey, W. A. Rutala, D. J. Weber, and M. Sobsey, "Virus transfer from personal protective equipment to healthcare employees' skin and clothing," *Emerg. Infect. Dis.*, vol. 14, no. 8, pp. 1291–1293, Aug. 2008.

[22] L. Casanova, W. A. Rutala, D. J. Weber, and M. D. Sobsey, "Coronavirus Survival on Healthcare Personal Protective Equipment," *Infect. Control Hosp. Epidemiol.*, vol. 31, no. 5, pp. 560–561, 2010.

[23] R. Mittal, R. Ni, and J. H. Seo, "The flow physics of COVID-19," *J. Fluid Mech.*, vol. 894, p. F2, Jul. 2020.

[24] S. Peng, Q. Chen, and E. Liu, "The role of computational fluid dynamics tools on investigation of pathogen transmission: Prevention and control," *Science of the Total Environment*, vol. 746. 2020.

[25] R. Blossey, "Self-cleaning surfaces - Virtual realities," *Nat. Mater.*, vol. 2, no. 5, pp. 301–306, 2003.

[26] C. Korte and A. M. Jacobi, "Condensate retention effects on the performance of plain-fin-and-tube heat exchangers: Retention data and modeling," *J. Heat Transfer*, vol. 123, no. 5, pp. 926–936, 2001.

[27] E. D. Wilkes and O. A. Basaran, "Forced oscillations of pendant (sessile) drops," *Phys. Fluids*, vol. 9, no. 6, pp. 1512–1528, 1997.

[28] J. Chatterjee, "A criterion for buoyancy induced drop detachment based on an analytical approximation of the drop shape," *Colloids Surfaces A Physicochem. Eng. Asp.*, vol. 178, no. 1–3, pp. 249–263, 2001.

[29] Y. S. Shin and H. C. Lim, "Shape oscillation and detachment conditions for a droplet on a vibrating flat surface," *Eur. Phys. J. E*, vol. 37, no. 8, pp. 1–10, 2014.

[30] P. Sartori *et al.*, "Drop motion induced by vertical vibrations," *New J. Phys.*, vol. 17, no.

11, 2015.

[31] S. C. Fu, Y. S. Cheung, H. H. Lee, J. K. C. Kwan, and C. Y. H. Chao, "Studies on detachment behavior of micron sized droplets: A comparison between pure fluid and nanofluid," *Aerosol Sci. Technol.*, vol. 52, no. 1, pp. 69–77, Jan. 2018.

[32] Y. Sui, H. Ding, and P. D. M. Spelt, "Numerical simulations of flows with moving contact lines," *Annu. Rev. Fluid Mech.*, vol. 46, pp. 97–119, 2014.

[33] J. Lee, S. W. Son, M. Y. Ha, and H. R. Kim, "A numerical study on the dynamic behavior of the liquid located between pillar-shaped structures," *J. Mech. Sci. Technol.*, vol. 28, no. 10, pp. 4221–4232, 2014.

[34] M. Sbragaglia *et al.*, "Sliding drops across alternating hydrophobic and hydrophilic stripes," *Phys. Rev. E - Stat. Nonlinear, Soft Matter Phys.*, vol. 89, no. 1, 2014.

[35] C. Semprebon and M. Brinkmann, "On the onset of motion of sliding drops," *Soft Matter*, vol. 10, no. 18, pp. 3325–3334, 2014.

[36] X. P. Wang, T. Qian, and P. Sheng, "Moving contact line on chemically patterned surfaces," *J. Fluid Mech.*, vol. 605, pp. 59–78, 2008.

[37] J. B. Dupont and D. Legendre, "Numerical simulation of static and sliding drop with contact angle hysteresis," *J. Comput. Phys.*, vol. 229, no. 7, pp. 2453–2478, 2010.

[38] J. A. Otter, C. Donskey, S. Yezli, S. Douthwaite, S. D. Goldenberg, and D. J. Weber, "Transmission of SARS and MERS coronaviruses and influenza virus in healthcare settings: The possible role of dry surface contamination," *Journal of Hospital Infection*, vol. 92, no. 3. W.B. Saunders Ltd, pp. 235–250, Mar-2016.

[39] N. M. Wilson, A. Norton, F. P. Young, and D. W. Collins, "Airborne transmission of severe acute respiratory syndrome coronavirus-2 to healthcare workers: a narrative review," *Anaesthesia*, vol. 75, no. 8, pp. 1086–1095, 2020.

[40] P. F. Horve *et al.*, "Building upon current knowledge and techniques of indoor microbiology to construct the next era of theory into microorganisms, health, and the built environment," *Journal of Exposure Science and Environmental Epidemiology*, vol. 30, no. 2. Springer Nature, pp. 219–235, Mar-2020.

[41] S. W. X. Ong *et al.*, "Air, Surface Environmental, and Personal Protective Equipment Contamination by Severe Acute Respiratory Syndrome Coronavirus 2 (SARS-CoV-2)

from a Symptomatic Patient," *JAMA - Journal of the American Medical Association*, vol. 323, no. 16. American Medical Association, pp. 1610–1612, Apr-2020.

[42] Y. Liu *et al.*, "Aerodynamic Characteristics and RNA Concentration of SARS-CoV-2 Aerosol in Wuhan Hospitals during COVID-19 Outbreak," *bioRxiv*, vol. 86, no. 21, p. 2020.03.08.982637, 2020.

[43] C. Poirier *et al.*, "The Role of Environmental Factors on Transmission Rates of the COVID-19 Outbreak: An Initial Assessment in Two Spatial Scales.," *SSRN Electron. J.*, 2020.

[44] W. Luo *et al.*, "The role of absolute humidity on transmission rates of the COVID-19 outbreak," *medRxiv*. p. 2020.02.12.20022467, 2020.

[45] P. Shi *et al.*, "The impact of temperature and absolute humidity on the coronavirus disease 2019 (COVID-19) outbreak - evidence from China," *medRxiv*, p. 2020.03.22.20038919, 2020.

[46] M. R. Pendar and J. C. Páscoa, "Numerical modeling of the distribution of virus carrying saliva droplets during sneeze and cough," *Phys. Fluids*, vol. 32, no. 8, 2020.

[47] R. Bhardwaj and A. Agrawal, "Likelihood of survival of coronavirus in a respiratory droplet deposited on a solid surface," *Phys. Fluids*, vol. 32, no. 6:061704, 2020.

[48] R. Bhardwaj and A. Agrawal, "Tailoring surface wettability to reduce chances of infection of COVID-19 by a respiratory droplet and to improve the effectiveness of personal protection equipment," *Physics of Fluids*, vol. 32, no. 8:081702. 2020.

[49] G. Kampf, D. Todt, S. Pfaender, and E. Steinmann, "Persistence of coronaviruses on inanimate surfaces and their inactivation with biocidal agents," *Journal of Hospital Infection*, vol. 104, no. 3. pp. 246–251, 2020.

[50] J. M. Stauber, S. K. Wilson, B. R. Duffy, and K. Sefiane, "Evaporation of droplets on strongly hydrophobic substrates," *Langmuir*, vol. 31, no. 12, pp. 3653–3660, 2015.

[51] J. M. Stauber, S. K. Wilson, B. R. Duffy, and K. Sefiane, "On the lifetimes of evaporating droplets with related initial and receding contact angles," *Phys. Fluids*, vol. 27, no. 12, 2015.

[52] I. G. Currie, *Fundamental mechanics of fluids: Fourth edition*. 2016.

[53] C. W. Hirt and B. D. Nichols, "Volume of fluid (VOF) method for the dynamics of free

boundaries," *J. Comput. Phys.*, vol. 39, no. 1, pp. 201–225, 1981.

[54] J. U. Brackbill, D. B. Kothe, and C. Zemach, "A continuum method for modeling surface tension," *J. Comput. Phys.*, vol. 100, no. 2, pp. 335–354, 1992.

[55] M. A. Delele *et al.*, "Predicting the dynamic impact behaviour of spray droplets on flat plant surfaces," *Soft Matter*, vol. 12, no. 34, pp. 7195–7211, 2016.

[56] F. Fu, P. Li, K. Wang, and R. Wu, "Numerical Simulation of Sessile Droplet Spreading and Penetration on Porous Substrates," *Langmuir*, vol. 35, no. 8, pp. 2917–2924, 2019.

[57] J. Thalackottore Jose and J. F. Dunne, "Numerical simulation of single-droplet dynamics, vaporization, and heat transfer from impingement onto static and vibrating surfaces," *Fluids*, vol. 5, no. 4, 2020.

[58] M. Kumar and R. Bhardwaj, "A combined computational and experimental investigation on evaporation of a sessile water droplet on a heated hydrophilic substrate," *Int. J. Heat Mass Transf.*, vol. 122, pp. 1223–1238, 2018.

[59] D. C. D. Roux and J. J. Cooper-White, "Dynamics of water spreading on a glass surface," *J. Colloid Interface Sci.*, vol. 277, no. 2, pp. 424–436, 2004.

[60] G. I. Mantanis and R. A. Young, "Wetting of wood," *Wood Sci. Technol.*, vol. 31, no. 5, pp. 339–353, 1997.

[61] S. Chandra and C. T. Avedisian, "On the collision of a droplet with a solid surface," *Proc. R. Soc. A Math. Phys. Eng. Sci.*, vol. 432, no. 1884, pp. 13–41, 1991.

[62] Y. L. Hsieh, J. Thompson, and A. Miller, "Water Wetting and Retention of Cotton Assemblies as Affected by Alkaline and Bleaching Treatments," *Text. Res. J.*, vol. 66, no. 7, pp. 456–464, 1996.

[63] S. J. Jang, S. S. Baek, J. Y. Kim, and S. H. Hwang, "Preparation and adhesion performance of transparent acrylic pressure sensitive adhesives for touch screen panel," *J. Adhes. Sci. Technol.*, vol. 28, no. 19, pp. 1990–2000, 2014.

[64] A. John *et al.*, "Scalable In-hospital Decontamination of N95 Filtering Facepiece Respirator with a Peracetic Acid Room Disinfection System," *Infect. Control Hosp. Epidemiol.*, 2020.

[65] K. M. McGinty and W. J. Brittain, "Hydrophilic surface modification of poly(vinyl chloride) film and tubing using physisorbed free radical grafting technique," *Polymer*

(Guildf)., vol. 49, no. 20, pp. 4350–4357, 2008.

[66] S. V. Patankar and D. B. Spalding, "A calculation procedure for heat, mass and momentum transfer in three-dimensional parabolic flows," *Int. J. Heat Mass Transf.*, vol. 15, no. 10, pp. 1787–1806, 1972.

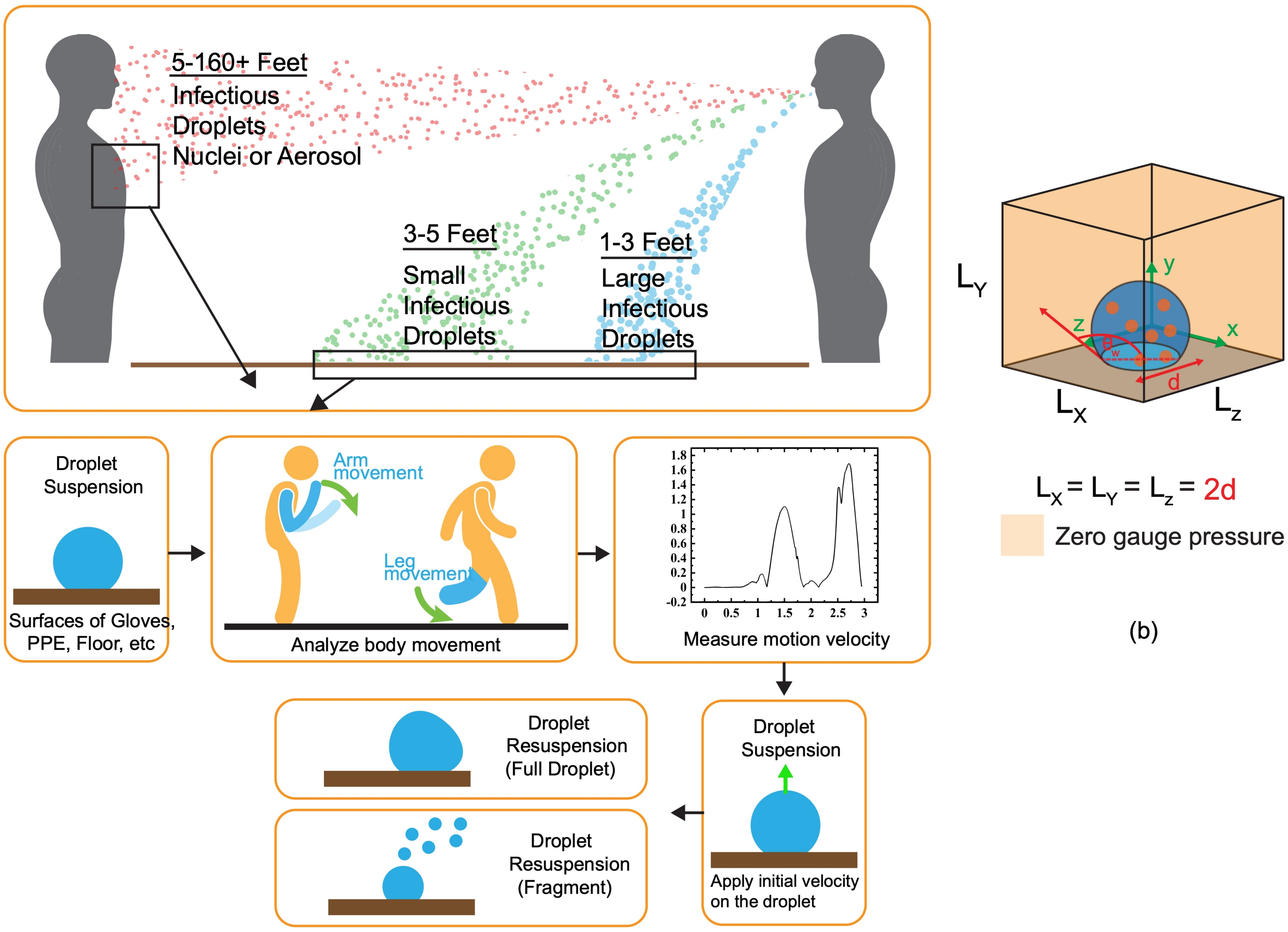
5-160+ Feet
Infectious
Droplets
Nuclei or Aerosol
3-5 Feet
Small
Infectious
Droplets
1-3 Feet
Large
Infectious
Droplets
Droplet
Suspension
Surfaces of Gloves,
PPE, Floor, etc
Arm
movement
Leg
movement
Analyze body movement
Measure motion velocity
Droplet
Suspension
Apply initial velocity
on the droplet
Droplet
Resuspension
(Full Droplet)
Droplet
Resuspension
(Fragment)
L_Y
L_X
L_z
y
x
z
d
$L_X = L_Y = L_z = 2d$
Zero gauge pressure
(b)

(a)

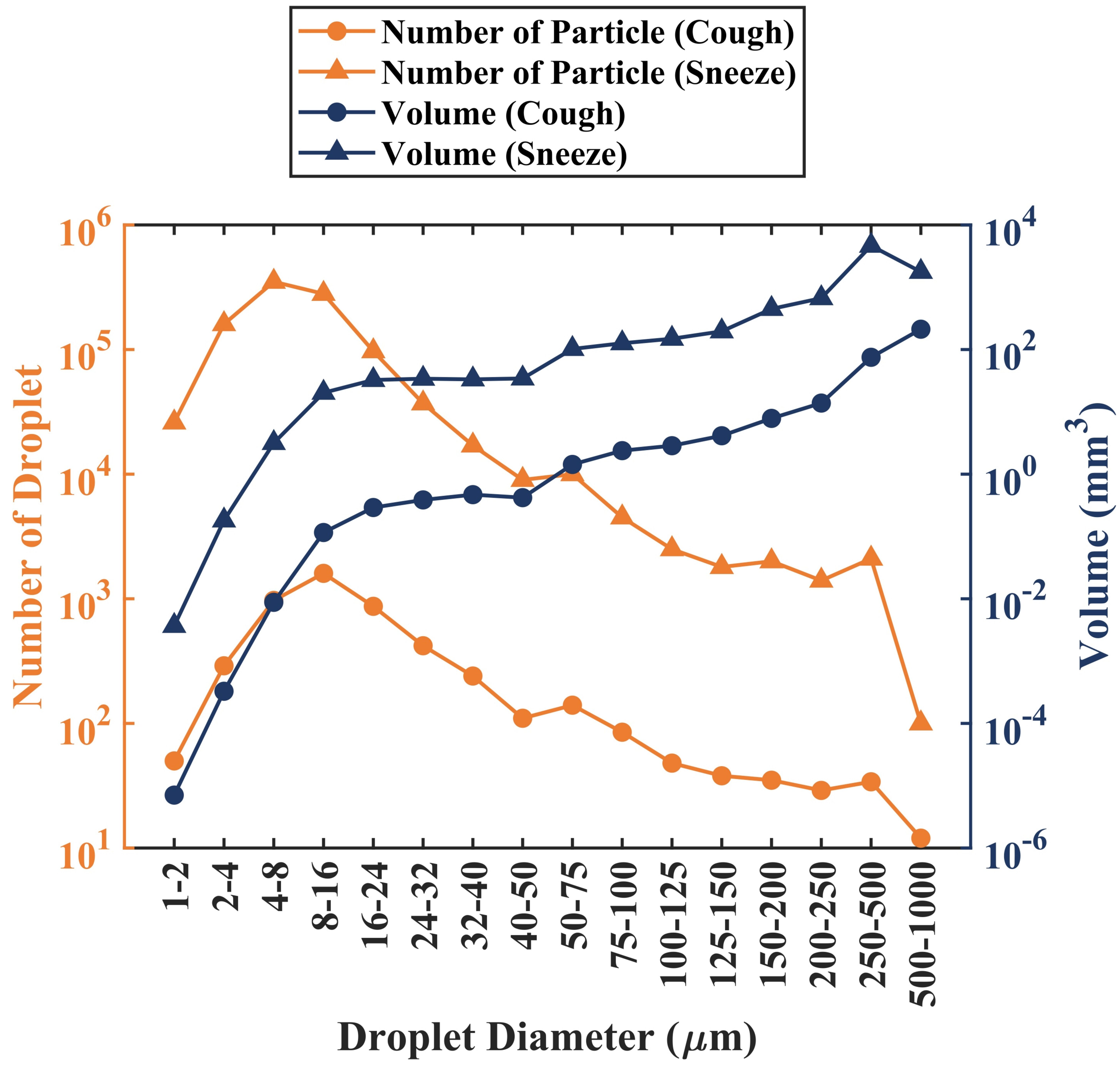

Number of Particle (Cough)
Number of Particle (Sneeze)
Volume (Cough)
Volume (Sneeze)
Number of Droplet
Volume (mm^3)
Droplet Diameter (μm)
10^1
10^2
10^3
10^4
10^5
10^6
10^{-6}
10^{-4}
10^{-2}
10^0
10^2
10^4
1-2
2-4
4-8
8-16
16-24
24-32
32-40
40-50
50-75
75-100
100-125
125-150
150-200
200-250
250-500
500-1000

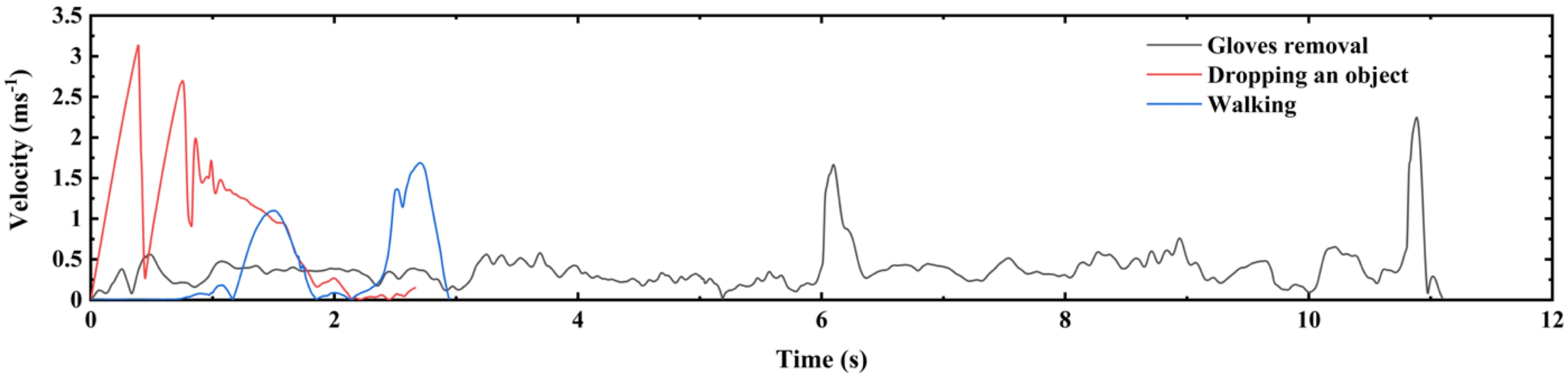
Gloves removal
Dropping an object
Walking
Velocity (ms^{-1})
Time (s)
0
0.5
1
1.5
2
2.5
3
3.5
0
2
4
6
8
10
12

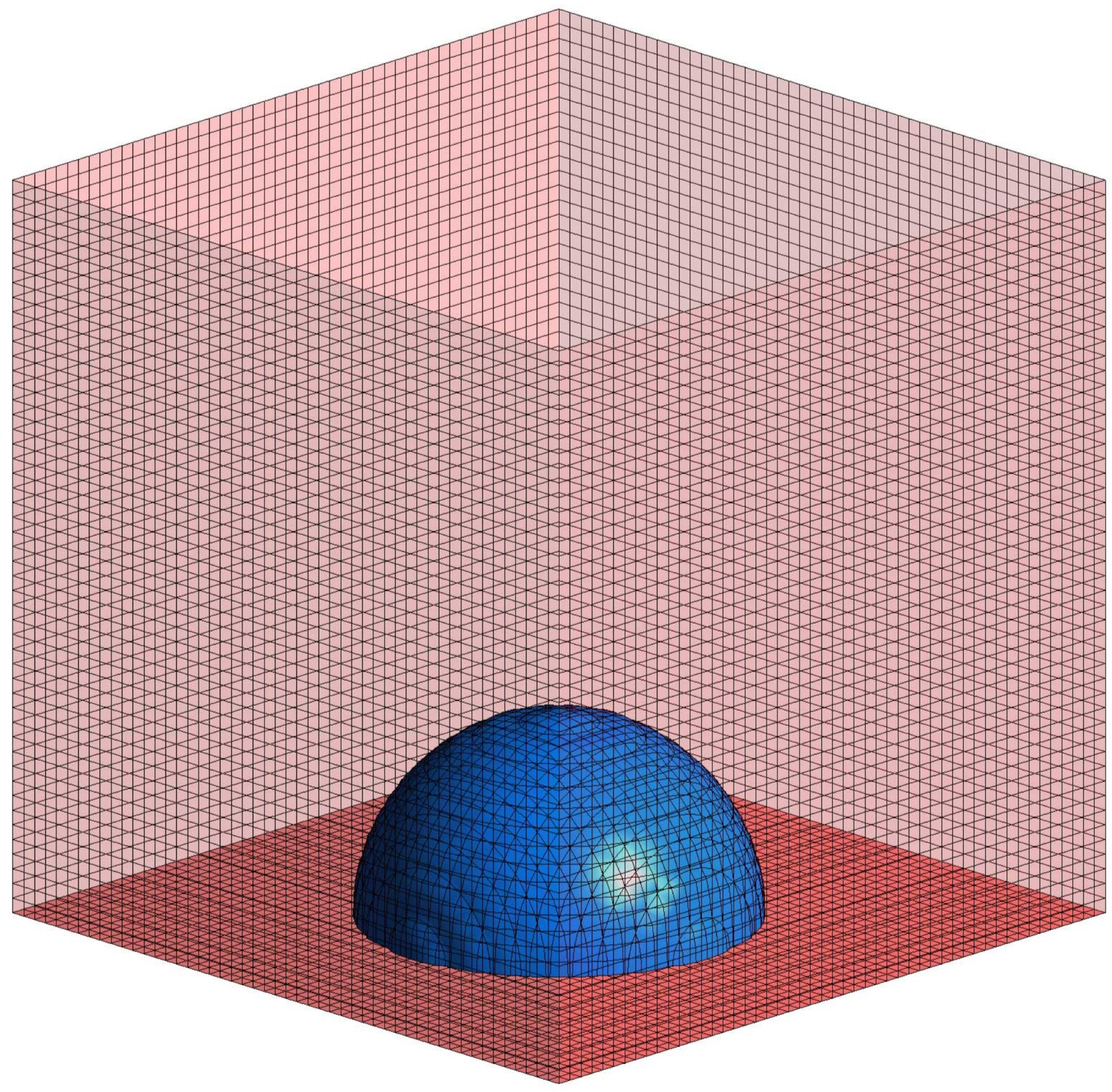

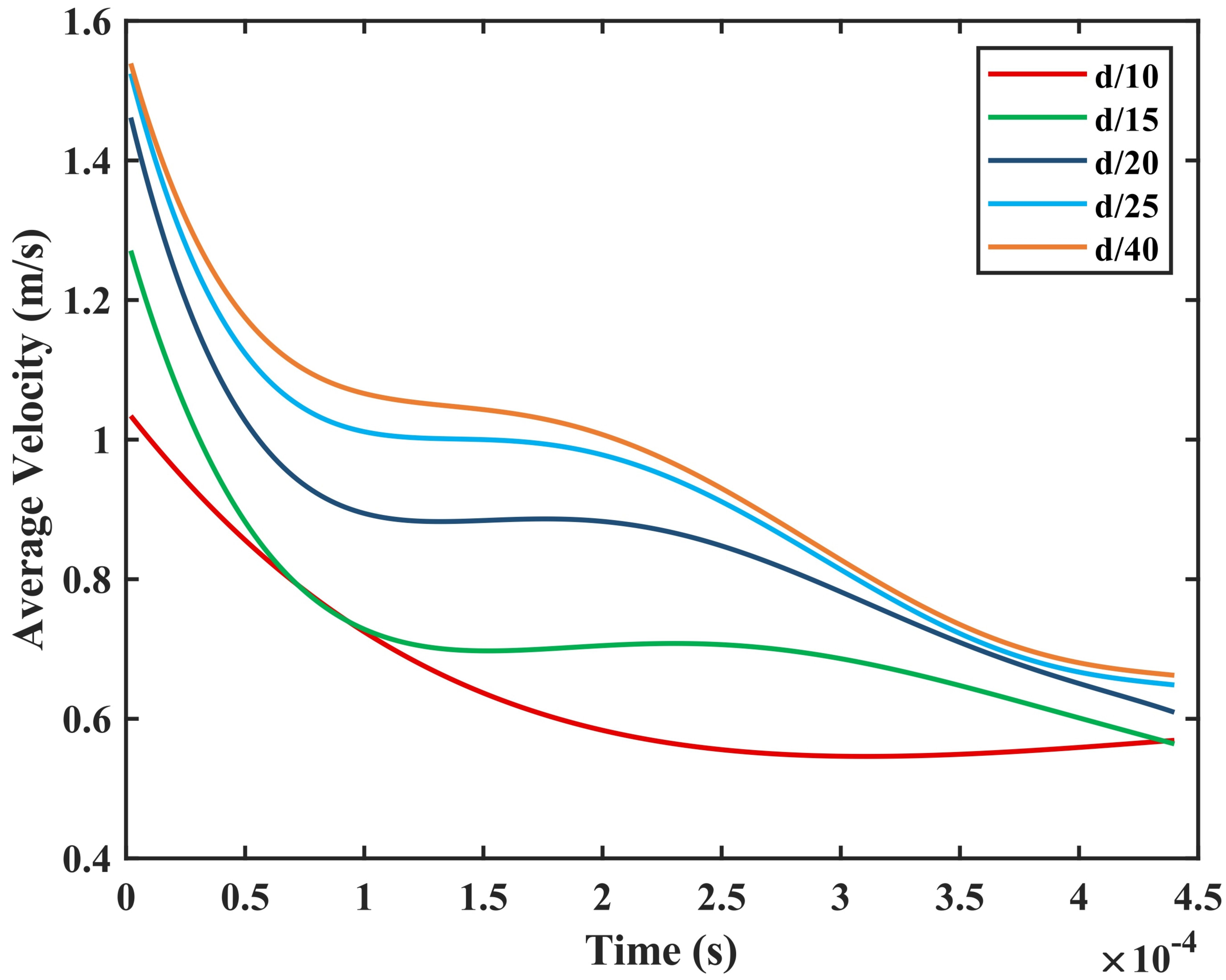
d/10
d/15
d/20
d/25
d/40
Average Velocity (m/s)
Time (s)
×10^-4
1.6
1.4
1.2
1
0.8
0.6
0.4
0
0.5
1
1.5
2
2.5
3
3.5
4
4.5

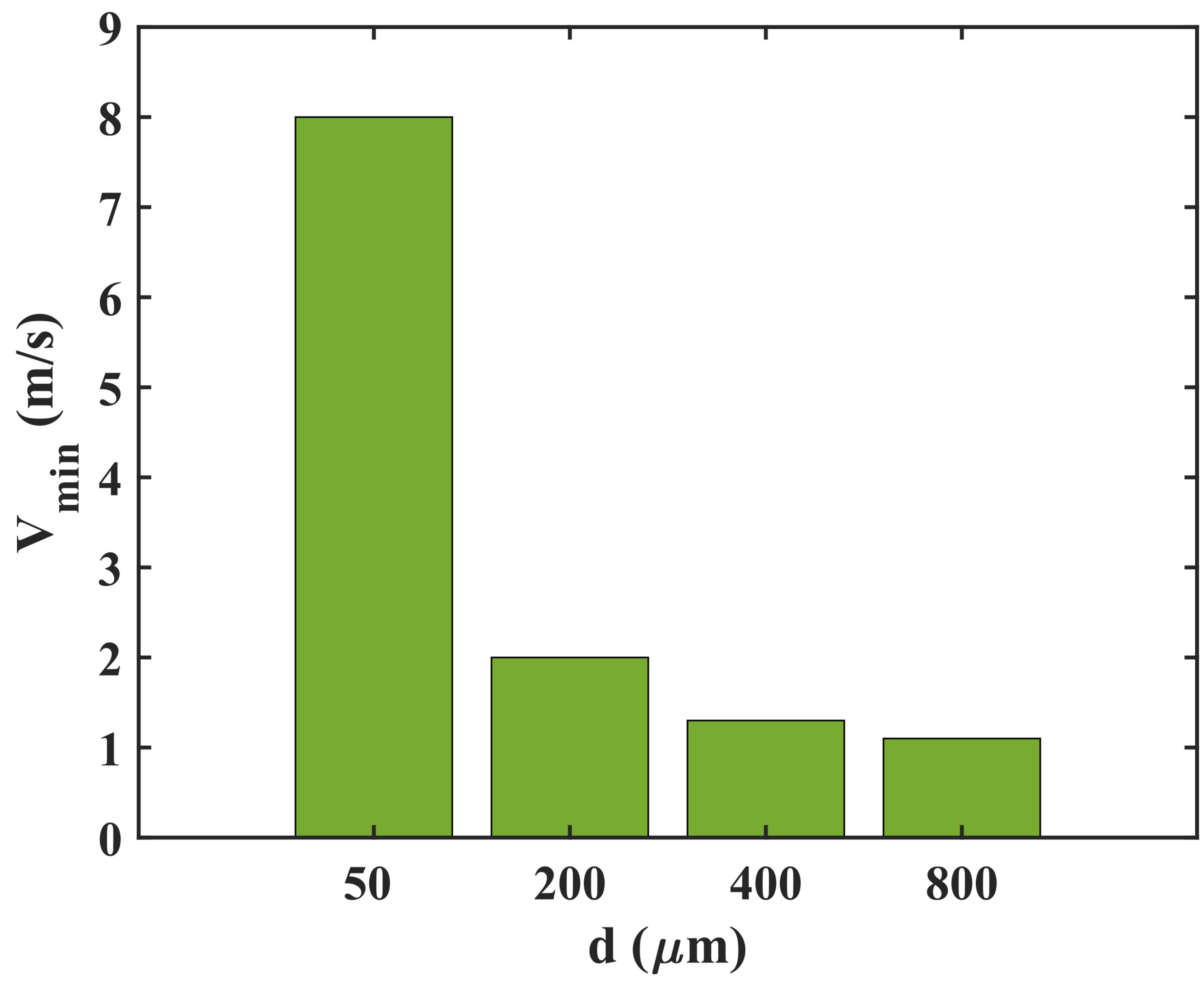

V_min (m/s)
0
1
2
3
4
5
6
7
8
9
50
200
400
800
d (μm)

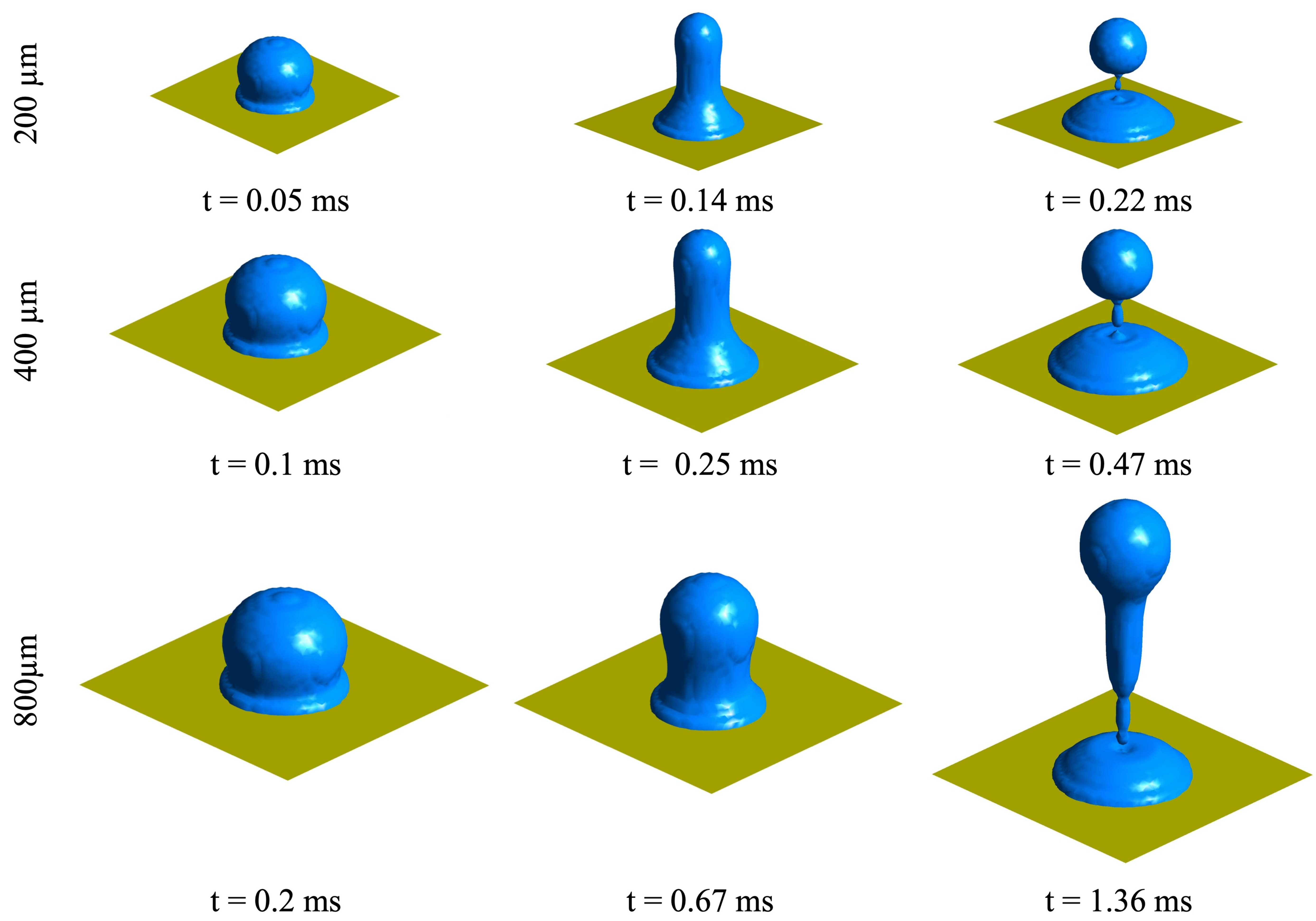
200 μm
t = 0.05 ms
t = 0.14 ms
t = 0.22 ms
400 μm
t = 0.1 ms
t = 0.25 ms
t = 0.47 ms
800μm
t = 0.2 ms
t = 0.67 ms
t = 1.36 ms

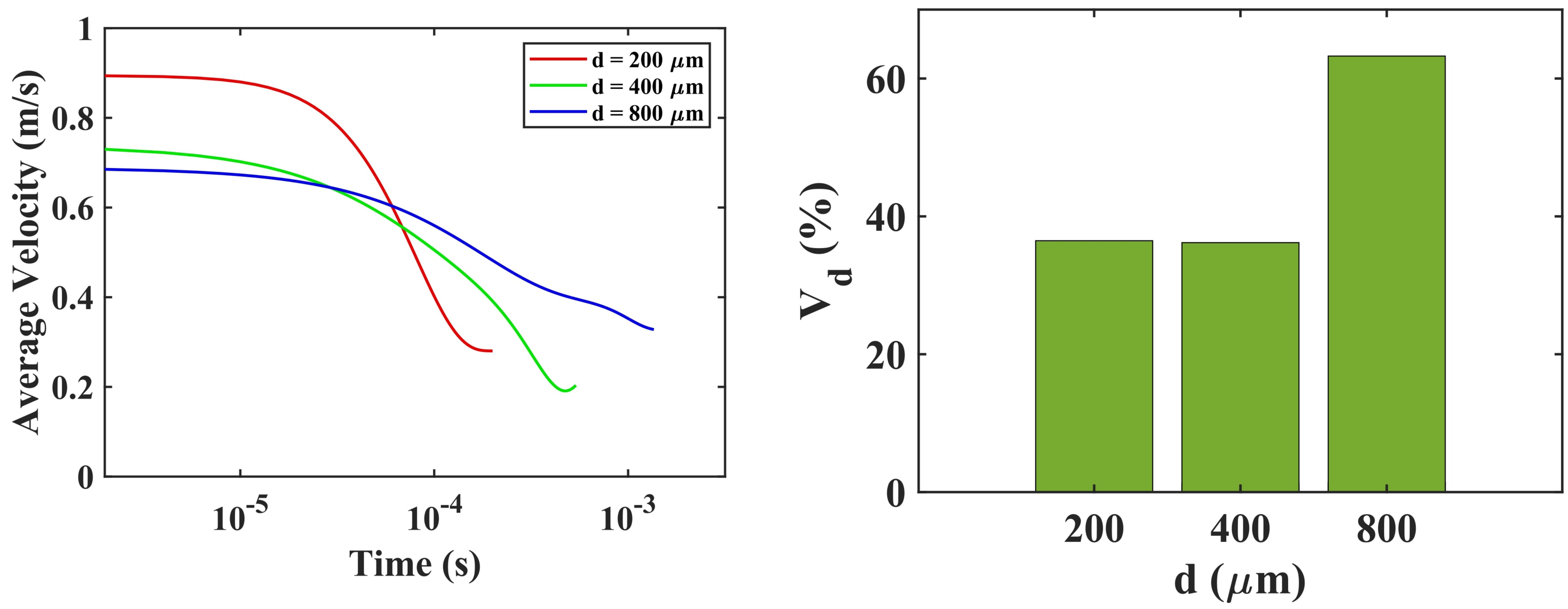
Average Velocity (m/s)
Time (s)
d = 200 μm
d = 400 μm
d = 800 μm
V_d (%)
d (μm)
200
400
800

(a) (b)

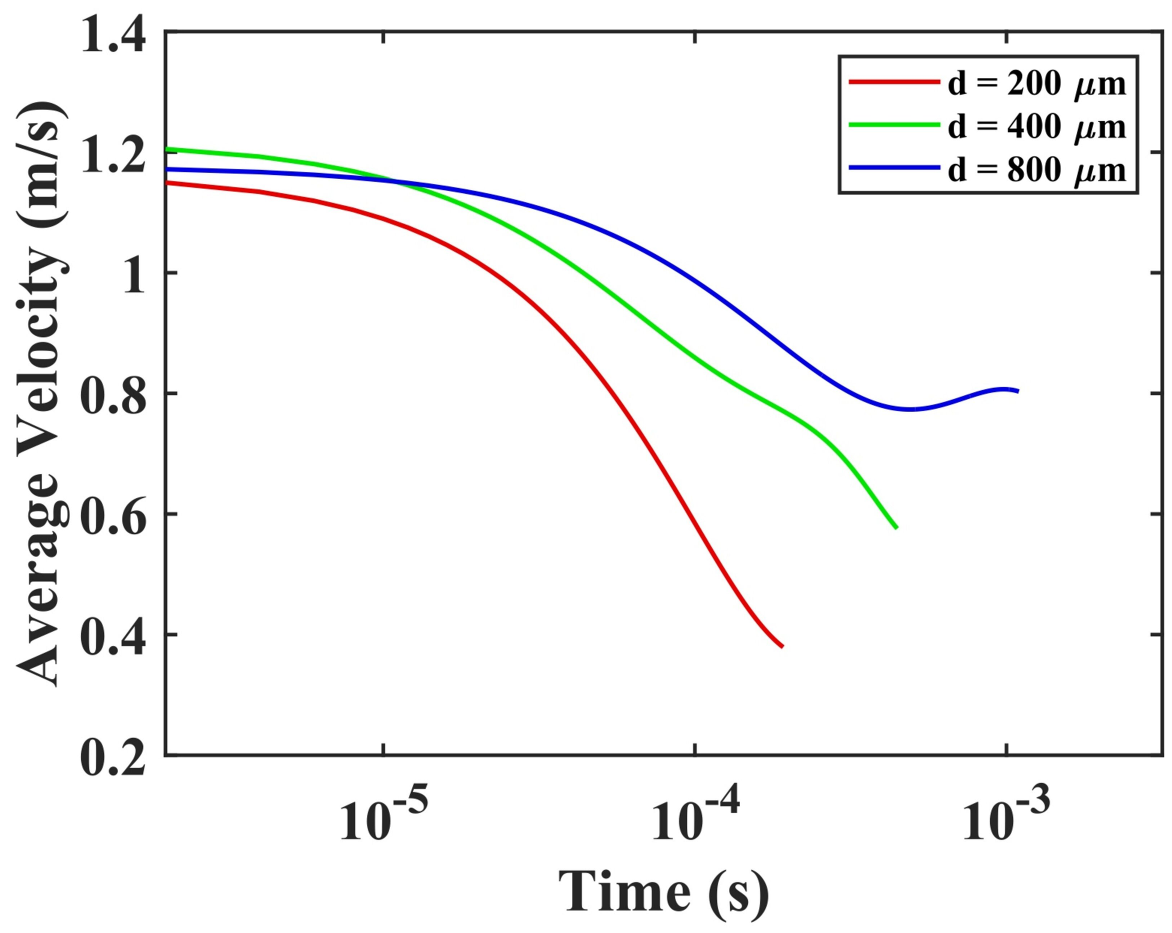

Average Velocity (m/s)
Time (s)
d = 200 μm
d = 400 μm
d = 800 μm

(a)

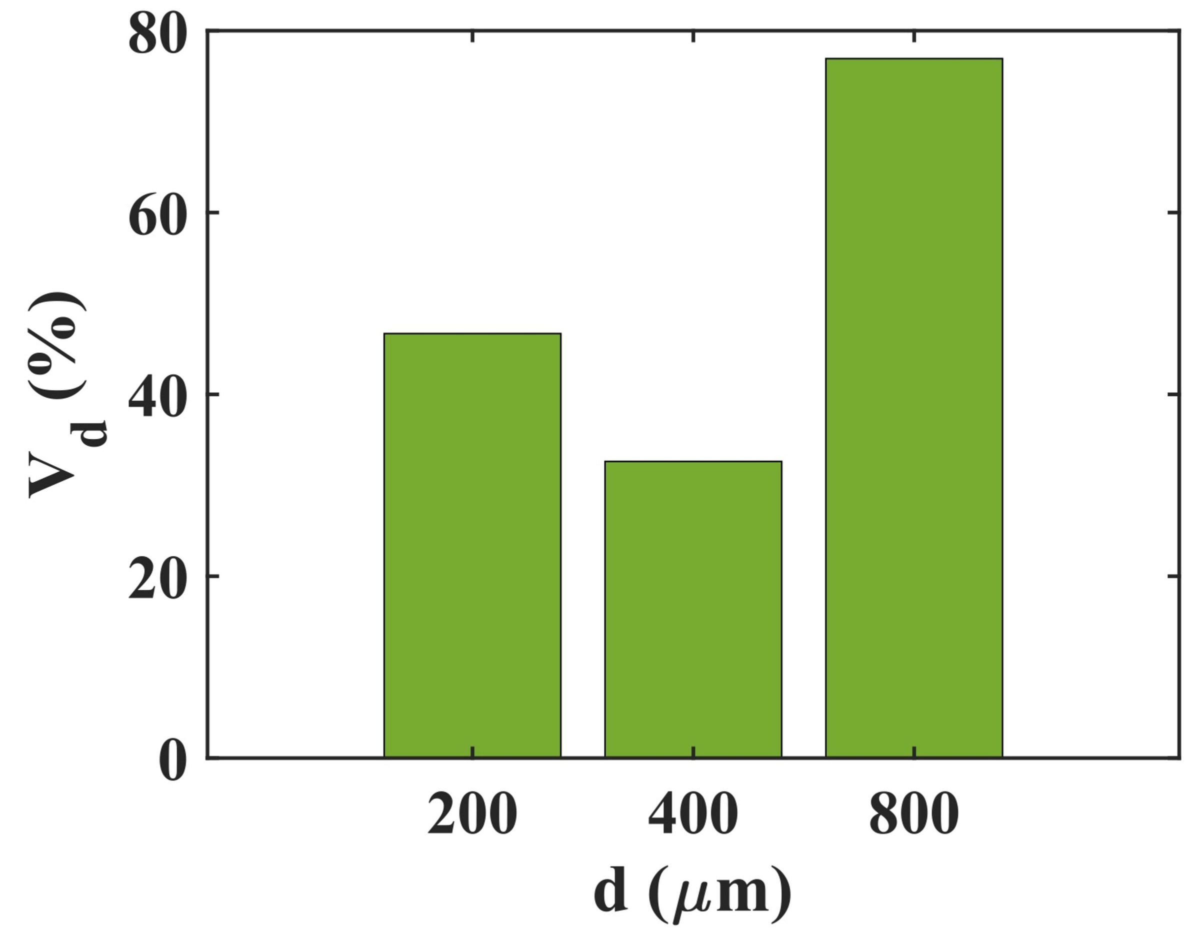

V_d (%)
d (μm)
200
400
800

(b)

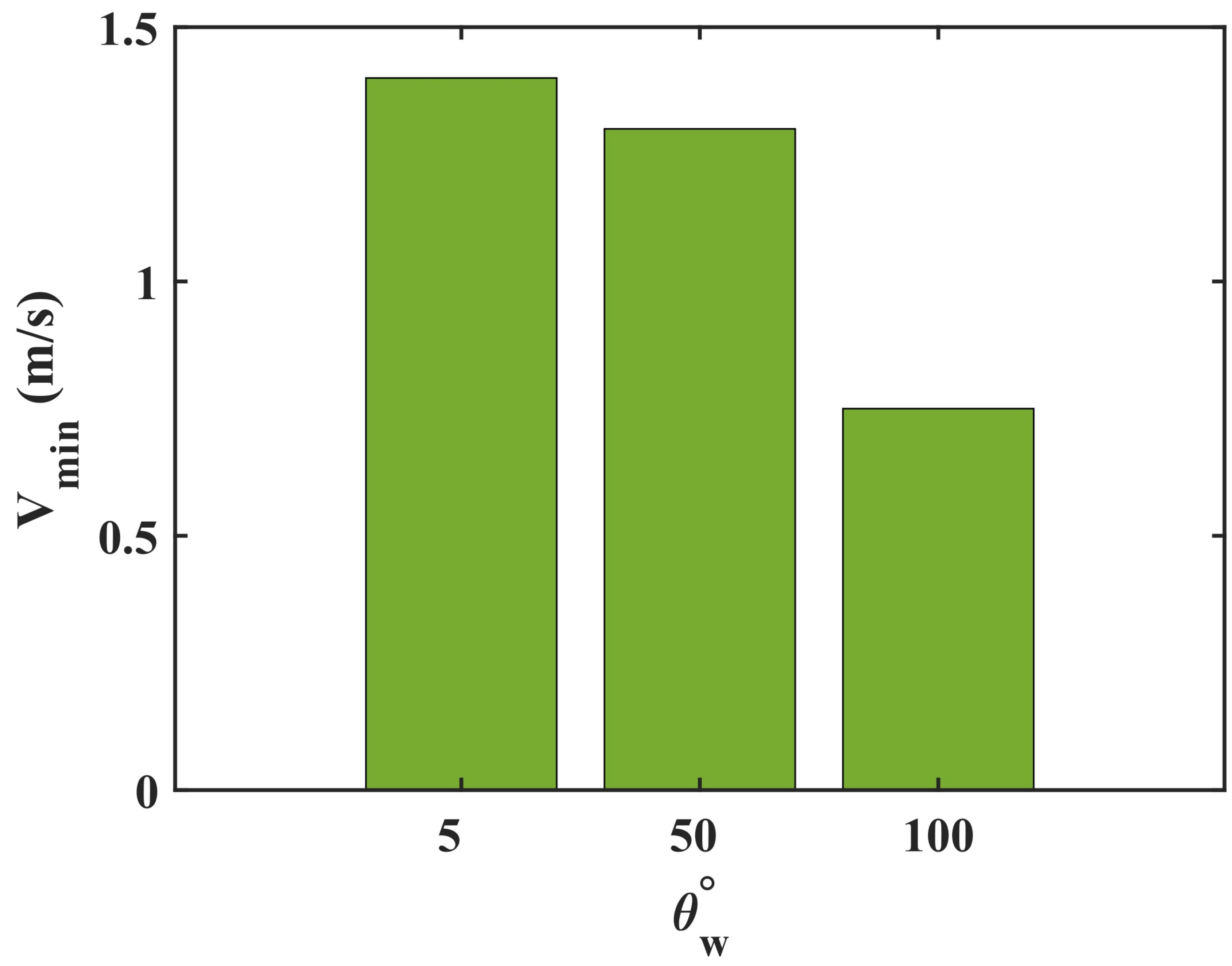
1.5
1
0.5
0
V min (m/s)
5
50
100
θ°w

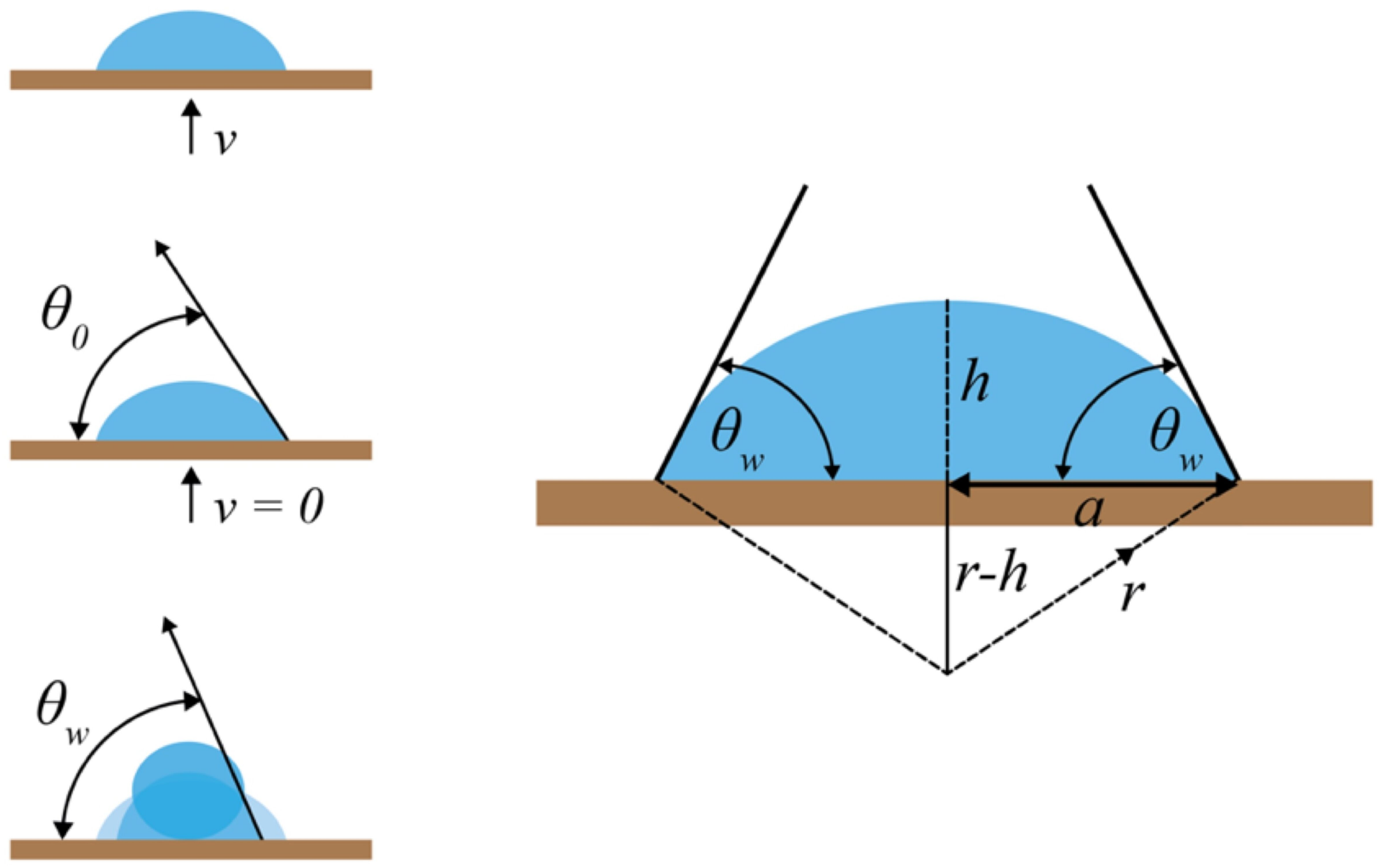

(a) (b)

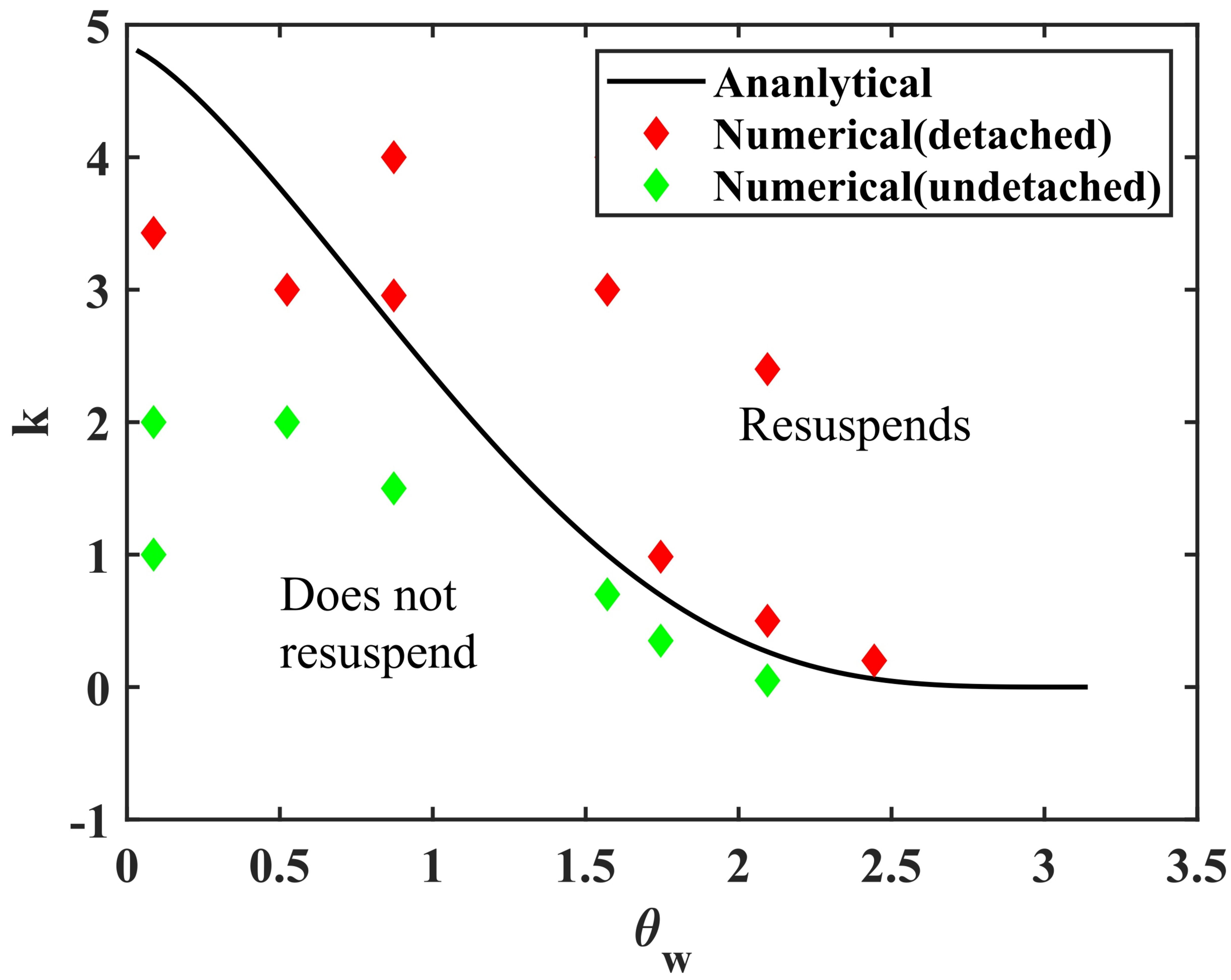
Ananlytical
Numerical(detached)
Numerical(undetached)
Resuspends
Does not
resuspend
k
θ_w
5
4
3
2
1
0
-1
0
0.5
1
1.5
2
2.5
3
3.5

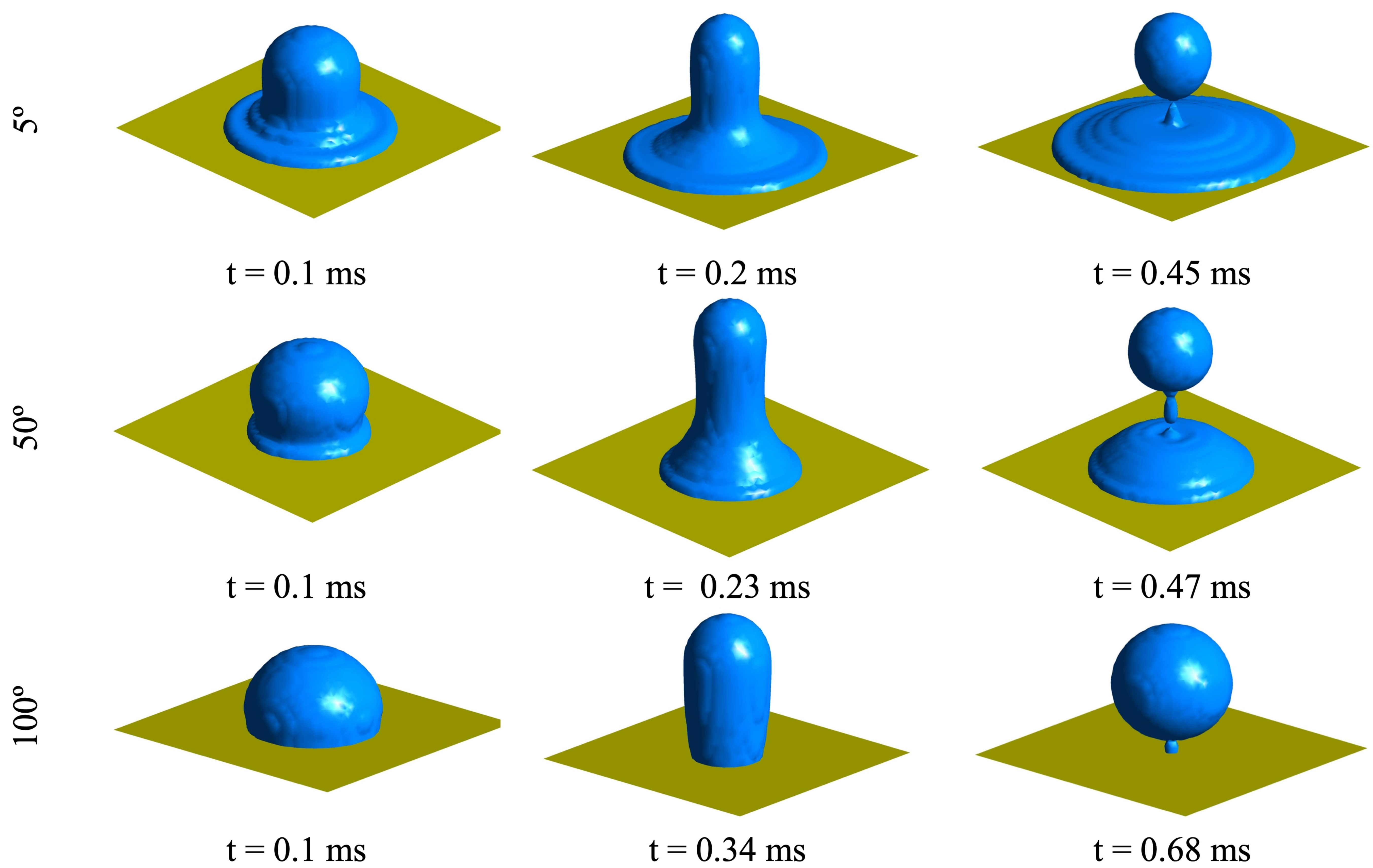
5º
t = 0.1 ms
t = 0.2 ms
t = 0.45 ms
50º
t = 0.1 ms
t = 0.23 ms
t = 0.47 ms
100º
t = 0.1 ms
t = 0.34 ms
t = 0.68 ms

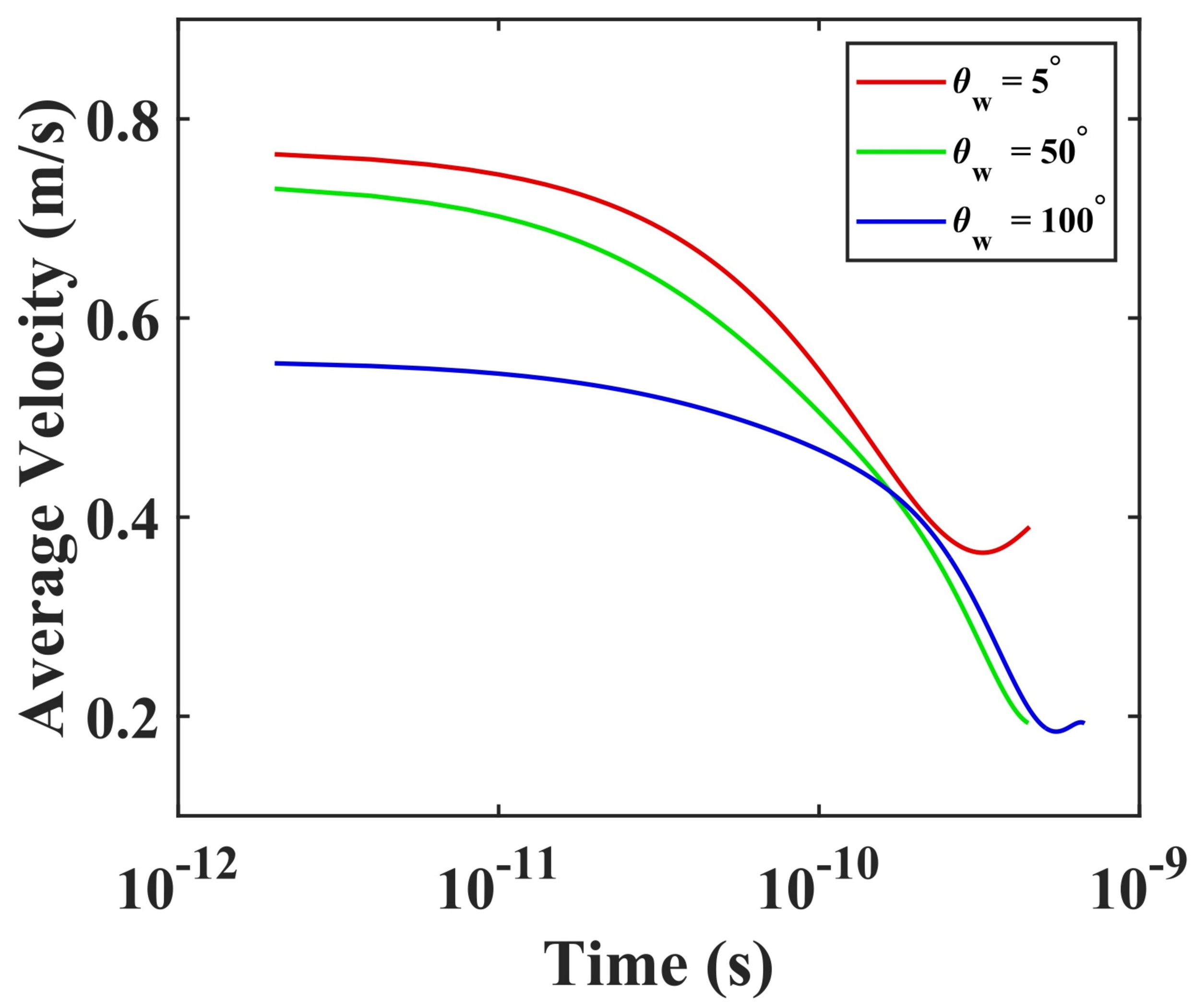

$\theta_w = 5^\circ$
$\theta_w = 50^\circ$
$\theta_w = 100^\circ$
Average Velocity (m/s)
0.8
0.6
0.4
0.2
10^{-12}
10^{-11}
10^{-10}
10^{-9}
Time (s)

(a)

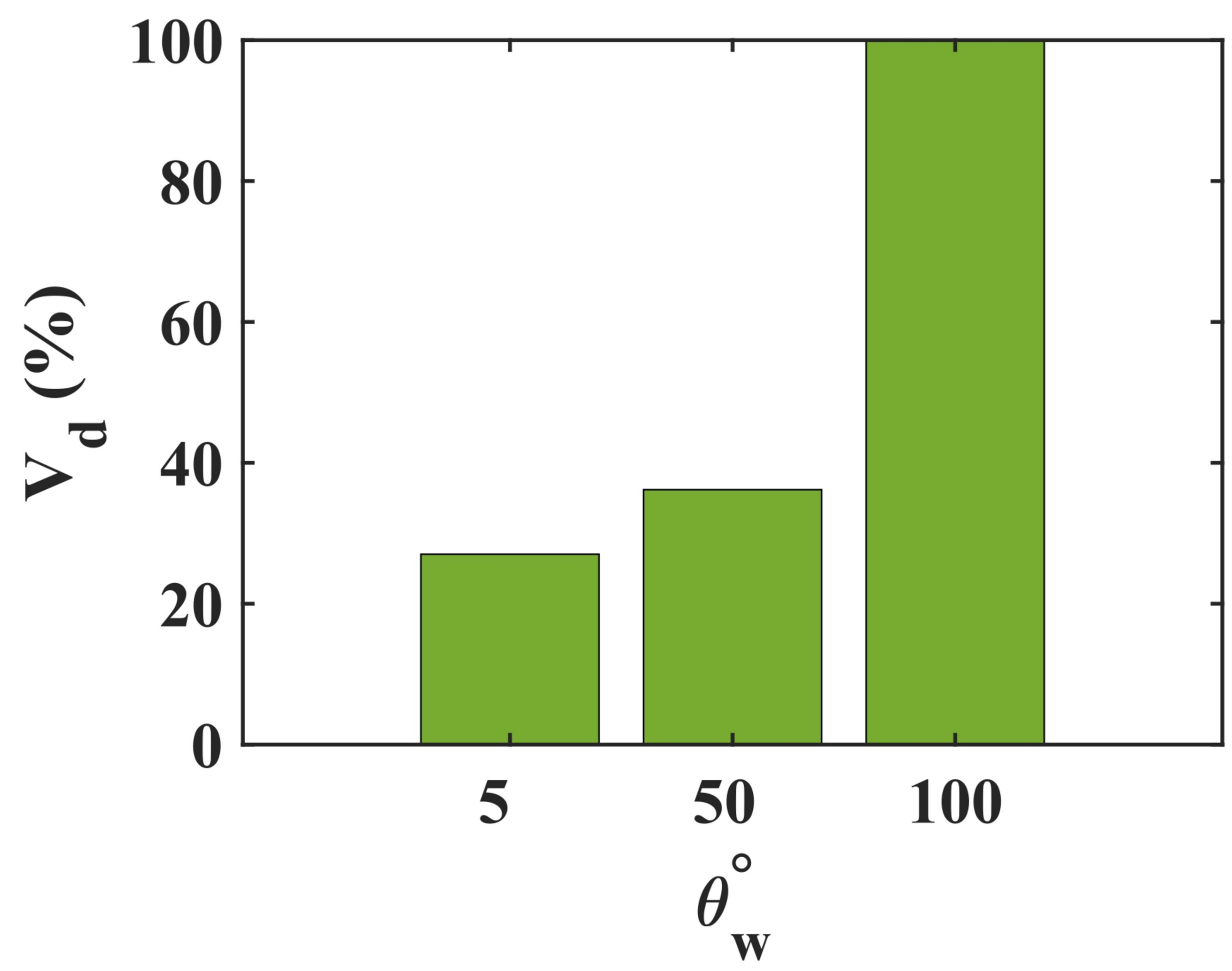

100
80
60
40
20
0
V_d (%)
5
50
100
θ_w°

(b)